Order in chaos: Structure of chaotic invariant sets of square-wave neuron models

Sergio Serrano,[1, a)] M. Angeles Martínez,[1, b)] and Roberto Barrio[1, c)]

Departamento de Matemática Aplicada and IUMA. University of Zaragoza. E-50009. Spain.

(Dated: 9 March 2021)

Bursting phenomena and, in particular, square-wave or fold/hom bursting, are found in a wide variety of mathematical neuron models. These systems have different behavior regimes depending on the parameters, whether spiking, bursting or chaotic. We study the topological structure of chaotic invariant sets present in square-wave bursting neuron models, first detailed using the Hindmarsh-Rose neuron model and later exemplary in the more realistic model of a leech heart neuron. We show that the unstable periodic orbits that form the skeleton of the chaotic invariant sets are deeply related with the spike-adding phenomena, typical from these models, and how there are specific symbolic sequences and a symbolic grammar that organize how and where the periodic orbits appear. Linking this information with the topological template analysis permits us to understand how the internal structure of the chaotic invariants is modified and how more symbolic sequences are allowed. Furthermore, the results allow us to conjecture that, for these systems, the limit template when the small parameter ε, which controls the slow gating variable, tends to zero is the complete Smale topological template.

Keywords: Low-dimensional chaos, neuron models, chaotic invariants, periodic orbits, topological template, bifurcations, symbolic dynamics, Hindmarsh-Rose model

[a)]Electronic mail: sserrano@unizar.es
[b)]Electronic mail: gelimc@unizar.es
[c)]Electronic mail: rbarrio@unizar.es

Deciphering how the brain works is one of the main challenges of science of this century. An important step in reaching this goal is a deep understanding of how neurons behave. Both at an experimental level and in mathematical models with square-wave bursting, it has been detected that neurons may have chaotic behavior. The bifurcations that organize the different types of bursting have been extensively studied in recent years. However, the structure of chaotic attractors has been much less researched. In fact, the different chaotic invariant sets (both attractors and saddles) and their evolution in parametric space has not been previously studied. This analysis is necessary because these invariant sets condition the dynamics (both chaotic and regular) of the neurons. It is well known that the unstable periodic orbits (UPOs) foliated to a chaotic invariant set constitute its dynamical skeleton[1], and with this information we can define the symbolic sequence of any orbit embedded in it. These symbolic sequences are organized according to a symbolic grammar that structures the existence of the different periodic orbits, both in the phase space and in the parameter space, that form the different chaotic invariant sets. As a prototype neuronal model, we use the Hindmarsh-Rose model, although we will show how analogous results are obtained in the leech heart neuron model. This suggests that these results are extensible to other neuron models with square-wave bursting behavior. Some of our results, related to the appearance of new symbolic chains in the spike-adding process, allow us to conjecture that the Smale topological template is completed at the limit when the small parameter (which controls the slow variable) tends to zero.

I. INTRODUCTION

In 1952, Hodgkin and Huxley published a mathematical model of the membrane current of a squid giant axon. It was the first mathematical model of a neuron, and 11 years later they received the Nobel Prize in medicine. Since then, numerous models (mostly modifications of the original one) have been developed and used to study the behavior of neurons from different animals. All these models can be studied and classified in the first instance through fast-slow decomposition[2,3]. This decomposition is based on the existence of fast and slow variables and two manifolds obtained in the limit case (when the slow variables are considered as constants, we obtain *the fast subsystem*) to which the orbits of the full model are attached. In the neuron models, the fast manifold is tubular (with open or closed ends) and the orbits move fast around it, later connecting with the slow manifold via some limit cycle bifurcation entering in a slow dynamics phase (see for more details Refs. 2 and 3). Each turn around the fast manifold is called a spike. When the movement performs several spikes before returning to the slow manifold, the dynamics are said to be of bursting type. Besides, it is well known that the dynamics of the neuron models can be chaotic[4–7], so, apart from classifying the regular bursting regimes, it is interesting to understand how chaotic behavior can appear in such systems, how this chaotic behavior is organized and how the spike-adding phenomena influence chaotic behavior. The type of bursting orbits that we will focus on in this article is the square-wave or fold/hom[8] bursting, so called because the limit cycles that make up the fast (tubular) manifold end abruptly in a homoclinic bifurcation of the fast subsystem. Here the orbit of the original system jumps to the slow manifold and leaves it at a fold bifurcation of the equilibria of the fast subsystem. This type of bursting is a common case in most neuron models and it has been observed that different models with this type of bursting present a region of the phase space with an alternation of chaotic and regular bands[9–11], and these are the ingredients we need in the analysis.

Last few years, several articles connect different bifurcations in the generation of the spike-adding phenomena and the chaotic attractors[9–13], but what is missing is to study in detail if there are differences among the chaotic invariant sets that appear in the complete parameter space of a neuron model. That is, looking at the regular behaviors we have different bursting behaviors with distinct number of spikes. Are there differences in the topology of the different chaotic invariant sets? How the spike-adding phenomena organize them? In order to answer these questions we use the symbolic dynamics techniques designed for strongly dissipative 3D systems[14–19]. This is not a great limitation since most neuron systems are strongly dissipative. As the contraction of the flow along the stable manifold is much greater than the expansion along the unstable manifold of equilibria[7,17], the Poincaré First Return Map (FRM) of the invariant chaotic sets can be obtained. These FRMs define one-dimensional maps that help in the characterization of the topological templates and allow the generation of symbolic dynamics. With these techniques, we will study (for the first time in the literature, as far as we know) the structure of both chaotic attractors and chaotic saddles. This analysis will allow us to understand the organization and evolution of both the chaotic dynamics and the skeleton of periodic orbits along the parametric region where such chaotic behavior exists.

In order to help in the analysis of neuron models simulated realistically within the Hodgkin-

Huxley framework[20], a common approach is to use some simplified models. In this paper we use as first step a reduced version of the conductance-based Hodgkin-Huxley model, the Hindmarsh-Rose (HR) model[21]:

$$\begin{cases} \dot{x} = y - ax^3 + bx^2 - z + I, \\ \dot{y} = c - dx^2 - y, \\ \dot{z} = \varepsilon[s(x - x_0) - z], \end{cases} \tag{1}$$

where x is the membrane potential, y the fast and z the slow gating variables for ionic current. Some parameters are typically set as follows: $a = 1$, $c = 1$, $d = 5$, $s = 4$, $x_0 = -1.6$. The remaining parameters b, I and ε (the small parameter which controls the slow gating variable) will be considered as bifurcation parameters. The dynamics are similar for most of the bursting models in the square-wave (or fold/hom) regime (as shown in Section V for the leech heart neuron model[22]).

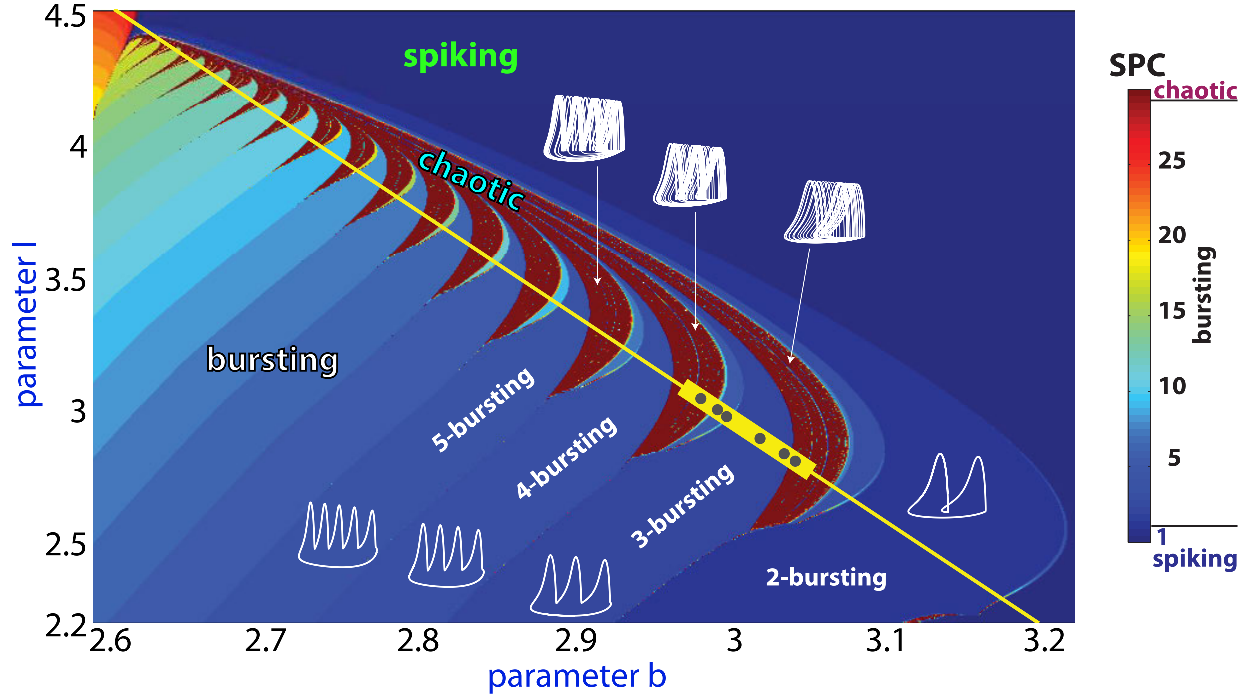

FIG. 1. (b, I)-biparametric sweep of the Hindmarsh-Rose model based on the spike-counting approach for $\varepsilon = 0.01$. The color-coded bar to the right gives the spike-number range. The white orbits represent 2D projections of typical attractors on the corresponding regions (abscissa corresponds to z variable and ordinate to x). We remark the yellow line defined by $I(b) = (1 - 0.265b)/0.0691$, that is going to be studied in detail in the paper, and the six points in the thick yellow segment that are analyzed in Fig. 4.

Initially, we fix $\varepsilon = 0.01$ and we use the Spike-Counting (SC) method[23] to obtain a first biparametric picture with a classification of the dynamics of the model inside the region with square-wave bursting. For each pair of the grid parameter values we integrate during a transient time, after that, we look for periodicity considering the maximum z value. Thus, in Figure 1, we can distinguish regions where the periodic attractor is spiking (dark blue) or bursting (different colors for different number of spikes), or by contrast, the attractor is chaotic (dark red). In some of those regions we show (in white) a standard attractor from that region. We can see how there are several chaotic stripes separated by regular bursting stripes with an increasing number of spikes from one strip to another. In view of this biparametric picture, first we are going to study in detail a line that crosses all these stripes to analyze in depth the origin of the changes that occur and then we will extend the results to the biparametric case. The selected line is defined by $I(b) = (1-0.265b)/0.0691$ and it is represented by the yellow straight line in Figure 1.

In several recent articles[9,11–13] different aspects of the dynamics of the HR model have been considered, but focusing mainly on the bifurcations of the periodic orbits. How the chaotic attractors (and chaotic saddles) evolve in the parametric phase space has not been investigated in detail in literature, just briefly in Ref. 24 where a first approach to the characterization of the chaotic attractors is done, but without explaining how the changes are organized and why. Therefore, the main goal of this paper is to present a complete study on how the chaotic invariant sets of the HR model evolve via a careful analysis of the process of opening the symbolic sequences of the allowed periodic orbits embedded on the system. This study allows us to conjecture how the topological template of these invariant chaotic sets tends towards the complete Smale template. However, this not only shed light on chaotic invariant sets, it also provides new results on how new orbits are generated in the chaotic spike-adding region[4] and on the interrelation between chaotic invariant sets and the periodic orbits that will end up being absorbed by these sets.

This paper is organized as follows: Section II introduces the basic definitions and results used on the symbolic dynamics, topological templates and FRM; Section III studies the symbolic dynamics and bifurcations on HR model; Section IV shows the location of the unstable periodic orbits, inside the chaotic invariant set, when the parameters change and presents a three-parameter study; Section V briefly explores the leech heart neuron model; Section VI presents a theoretical scenario of the way the chaotic invariant sets evolve towards the complete Smale horseshoe template in square-wave bursters; and finally, Section VII presents some conclusions.

II. SYMBOLIC DYNAMICS AND TOPOLOGICAL TEMPLATES

To characterize the behavior of a dynamical system, several theoretical and analytical tools have been introduced in literature, but most of them focus on classifying the observed behavior as regular or chaotic. When a chaotic behavior is observed, a first task is to know if this dynamics is due to a transient phenomenon or if we really have a chaotic attractor, having in both cases a chaotic invariant set (saddle or attractor). What is more difficult is to classify the different chaotic invariant sets and the structure of the skeleton of periodic orbits embedded in it. In this section we compile the basic definitions and results on the techniques that we will use in the subsequent study[18,19] and we make a first application to the HR model.

Given a suitable Poincaré section, we can define the First Return Map of an orbit as $FRM(x_n) = x_{n+1}$ where x_i are the values of the selected coordinate at the successive points of the Poincaré section of the orbit. On the HR model the FRM is calculated using the Poincaré section $x = 0$, with $\dot{x} > 0$, and selecting the z component, so the FRM shows the map (z_n, z_{n+1}). This Poincaré section generates a point for each spike that the orbit experiences. FRMs of the chaotic invariant sets on HR system are unimodal (see Figure 2(c)). Other more realistic biological models, like the leech heart neuron model, also present a unimodal FRM[22]. Note that, when the chaotic attractor exists, the FRM is obtained quite easily, but when there is a stable limit cycle coexisting with a chaotic saddle the problem is more complex numerically speaking. There are several numerical methods in literature to compute chaotic saddles. We use the "Sprinkle method"[25], that works well when the transient time is large, as in this case. This method takes a uniform grid of points located in the transient region (the behavior of its trajectory is chaotic for a long time). The orbits started at these points will be moving very close to the chaotic saddle for a while and then they will depart towards the periodic attractor. For each of these starting points we save the intermediate part of its trajectory. With all the trajectories saved we have a good approximation of the chaotic saddle and we can get its FRM.

Let PO^n be a periodic orbit with topological period n. Its FRM will have n points $\{p_i | i = 0, \dots, n-1\}$, and we can assign a symbolic value, $s_i =$"0" or "1", depending on which branch of the chaotic FRM the point p_i is (symbol "0" denoting the positive slope branch, symbol "1" the negative one). So, we can assign a symbolic sequence Σ to the orbit, $\Sigma(PO^n) = (s_0 s_1 \dots s_{n-1})^\infty$ where $s_i \in \{0,1\}$ and $(\cdot)^\infty$ represents the infinite repetitions of the substring of n symbols. Actually, any cycle of $\Sigma(PO^n)$, $\sigma^k\Sigma(PO^n) = (s_k s_{k+1} \dots s_{n-1} s_0 \dots s_{k-1})^\infty$ being σ the "shift operator", is also a symbolic sequence of that orbit. To obtain uniqueness in the representation and moreover make the subsequent study of the existing orbits easier, we have to start at the FRM point of the orbit furthest to the right (i.e., with the largest value of z). We will also define the (infinite) symbolic sequence Σ_c of the chaotic invariant set starting at the rightmost point of its FRM, this is called the *kneading sequence*[26] (equivalently, the critical point of the unimodal FRM is used instead in other references).

The *Topological Template* (or knot holder or branched manifold), was introduced by Birman and Williams[14,15] to describe the topological organization of the unstable periodic orbits (UPOs) into the Lorenz dynamical system. This tool has played a very important role in the theoretical analysis of the Lorenz system[16]. The topological template for a dissipative three-dimensional dynamical system is generated by projection of its flow, squeezing it along the stable direction and, thus, going from a three-dimensional flow to a two-dimensional branched manifold. In fact we construct a version of the dynamical system in the limit of infinite dissipation. This projection is performed while maintaining the relative positions of the periodic orbits. So, crosses are not created or destroyed between them. Thus, through the organization of the UPOs among themselves, the template provides information on the stretching and squeezing processes that generate the chaotic attractor[17,18].

A systematic procedure to calculate a topological template has been described in Refs. 17, 18, 27, and 28. Figure 2 shows schematically the complete process of topological analysis of the Hindmarsh-Rose model. The first thing we need is to obtain the low-period periodic orbits (in our case up to 5 spikes). Then, using topological periods (number of spikes) and linking numbers (number of turns one orbit makes around another[29]), we characterize the intertwining of these periodic orbits. The last step is to determine which is the simplest template that fits the previous characterization. For this last step there are two alternatives. The first one is to use the information that the FRM provides. In the case of HR, the FRM is unimodal (and therefore the symbolic dynamics is represented by two symbols), so its template will only need two branches. Similarly, to provide symbolic sequences to the periodic orbits of the dynamical system, we can assign a symbolic sequence to the periodic orbits in the template based on the branch of the template they pass through. Due to the properties of the topological templates, the periodic orbits embedded in the chaotic invariant set that have the same symbolic sequences as the periodic orbits of the template must also have the same topological invariants. From the symbolic sequences and the linking numbers of the periodic orbits, the template characteristic numbers can be obtained, determining

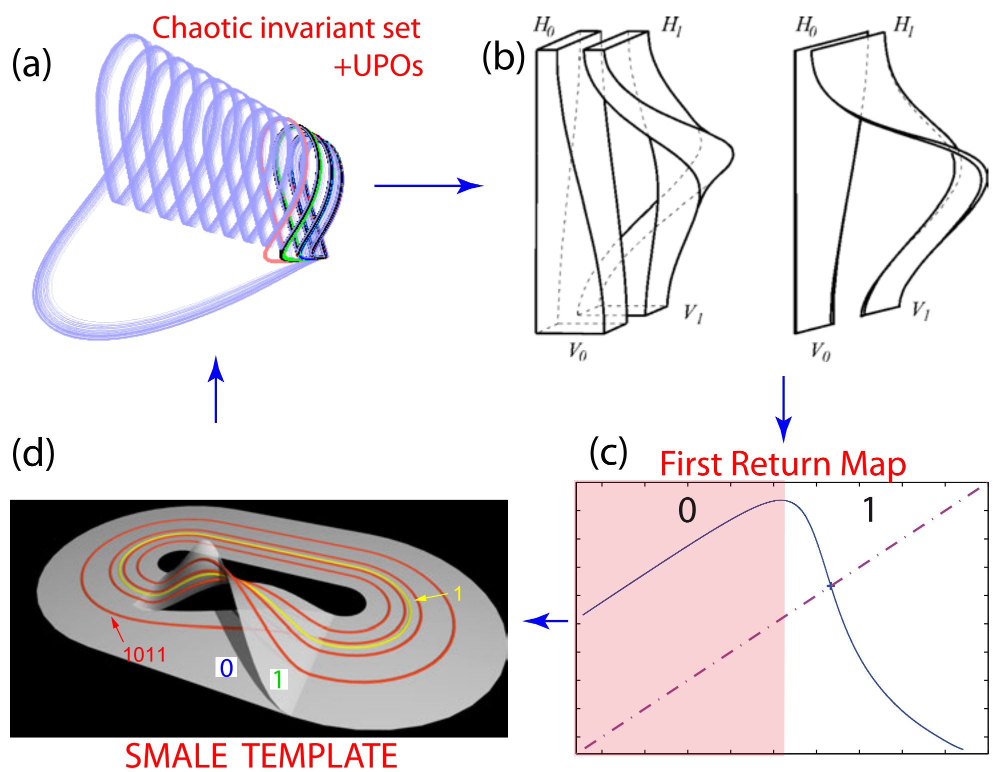

FIG. 2. Topological template analysis. (a) Chaotic invariant set and some foliated Unstable Periodic Orbits (UPOs). (b) Basis of the template analysis using the contraction direction. (c) First Return Map (FRM) of the invariant chaotic set and symbolic names of its branches. (d) Global template for the Hindmarsh-Rose model: Smale template. Each periodic orbit in the chaotic invariant set is related with a periodic orbit in the template.

therefore the template structure[18,30]. The second alternative does not use symbolic encoding. This algorithm calculates the topological invariants of all the possible symbolic names (starting with the simplest ones) of the orbits of the template until locating the set that makes these invariants coincide with those of the orbits of the dynamical system[18,31,32]. Actually, with this second algorithm, the symbolic sequences are obtained as a secondary final result. In our previous study[24] we followed both alternatives and obtained the same results with both. Therefore, the analysis carried out makes sense both from a topological and a dynamic point of view.

With the above process, we verified in[24] that the global topological template obtained in all cases was the Smale horseshoe template (see Fig. 2(d)). If the chaotic attractor is hyperbolic, all the orbits of the template exist in the attractor dynamics. If, as in our case, it is not hyperbolic, there are orbits in the template that do not exist in the dynamics of the chaotic attractor. But, the

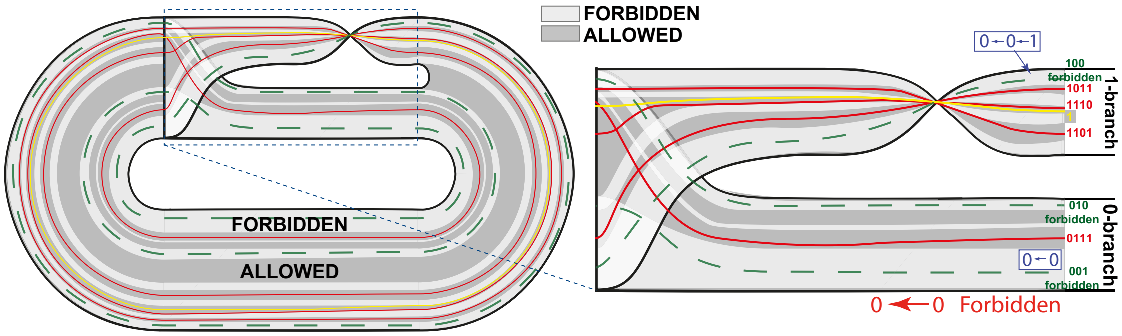

FIG. 3. Location of the forbidden symbolic sequences (illustrated the case of chain 00 forbidden) giving rise to a Cantor-like structure in the global template. The existing periodic orbits "1" and "1011" in the chaotic attractor are on the allowed "roads", while the "100" orbit is on the forbidden "roads", and therefore this orbit is not yet present in the chaotic invariant set.

existing orbits are organized within the template just as if the attractor were hyperbolic. Then, there are symbolic sequences of this template that do not appear within the chaotic invariant set. That is, the global template has certain closed lanes depending on the specific orbits that appear embedded in the chaotic set. The topological subtemplate reduced by these closed lanes has a Cantor structure, with holes caused by the symbolic sequences that do not appear (see Figure 3). If we look at the chaotic invariant set, we find a structure of the same type, where now the holes are originated by the orbits whose symbolic sequences are forbidden. In this way, the templates explain and classify the dynamics in the non-hyperbolic case. It is important to remark that, when the parameters change, there are orbits that appear or disappear following a certain order. In fact this is one of the main goals of this paper, to study how the HR system evolves towards the complete Smale template and how that evolution conditions the periodic orbits that appear. To describe this arrangement in the appearance (disappearance) of the periodic orbits, we will make use of the grammar of the symbolic sequences.

Firstly, let us establish an order relation in the set of the defined infinite symbolic sequences[18,19]. Given a finite symbolic sequence, S, we define

$$\rho(S) = \begin{cases} +1, & \text{if there is an even number of 1's in } S, \\ -1, & \text{if there is an odd number of 1's in } S. \end{cases} \tag{2}$$

Let $\Sigma = \Lambda s\ldots$ and $\Sigma' = \Lambda s'\ldots$ be two different symbolic sequences with a common leading symbolic string Λ and $s \neq s'$ the first different symbol from Σ and Σ', respectively. Then

$$\Sigma \prec \Sigma' \Leftrightarrow \rho(\Lambda s) = +1. \tag{3}$$

As an example, we show all possible periodic orbits up to period 5, with their corresponding order:

$$\begin{gathered} 0^\infty \prec 1^\infty \prec (10)^\infty \prec (1011)^\infty \prec (10111)^\infty \prec (10110)^\infty \prec (101)^\infty \prec (100)^\infty \\ (100)^\infty \prec (10010)^\infty \prec (10011)^\infty \prec (1001)^\infty \prec (1000)^\infty \prec (10001)^\infty \prec (10000)^\infty. \end{gathered} \tag{4}$$

Let's explain for example why $\Sigma = (10110)^\infty \prec \Sigma' = (101)^\infty$: $\Sigma = 1011010110...$ and $\Sigma' = 101101101...$, the common part $\Lambda = 101101$ and the first symbol after Λ is $s = 0$ for Σ (thus $\rho(\Lambda s) = +1$) and $s' = 1$ for Σ' (with $\rho(\Lambda s') = -1$). Therefore $\Sigma = (10110)^\infty \prec \Sigma' = (101)^\infty$. One can observe that the canonical symbolic element selected for a periodic orbit (considering as first point the rightmost one in the FRM) is the greatest, with this order, of all the possible symbolic sequences of that periodic orbit, that is, $\Sigma(PO_{canonical}) = \max_k\{\sigma^k\Sigma(PO_{canonical})\}$. For example, the period 4 periodic orbit $(1011)^\infty$ have other three different representations (see Fig. 3) with the corresponding ordination: $(0111)^\infty \prec (1101)^\infty \prec (1110)^\infty \prec (1011)^\infty$.

With this arrangement, a periodic orbit PO^n exists (is *admissible*) for some parameters, if $\Sigma(PO^n) \prec \Sigma_c$, with Σ_c the kneading sequence of the existing chaotic invariant set for those parameters[18]. If the chaotic set is an attractor, all UPOs embedded in the attractor are admissible. It is also clear that, given two periodic orbits PO_1^m and PO_2^n, if $PO_1^m \prec PO_2^n$ and PO_2^n is admissible, then also PO_1^m is admissible. So, the periodic orbits appear from smallest to largest with the order given by $\prec$. In turn, the dynamics of the chaotic set will include more symbolic sequences (approaching the Smale horseshoe template) the higher its kneading sequence Σ_c. This arrangement could be disturbed by the fact that the system is not infinitely dissipative[33]. However, all the studied orbits fit this arrangement (except 0^∞, which does not appear in the dynamics of the HR system). This symbolic dynamics is going to be one of the fundamental tools to describe, in the following sections, how and where the different periodic orbits appear, building the topological structure of the chaotic invariant sets.

Going back to the HR model, we begin this analysis in the regular window whose basic stable periodic orbit has 3 spikes. The corresponding interval is marked with a thick segment on the yellow straight line plotted in Figure 1. The gray points that appear there correspond to the values used in Figure 4. In that figure, we represent the FRM of the existing chaotic set (blue line) for each selected value. As we can see in Figure 1, for the first and last values the chaotic set is an attractor, while for the other values it is a saddle invariant set and no longer an attractor.

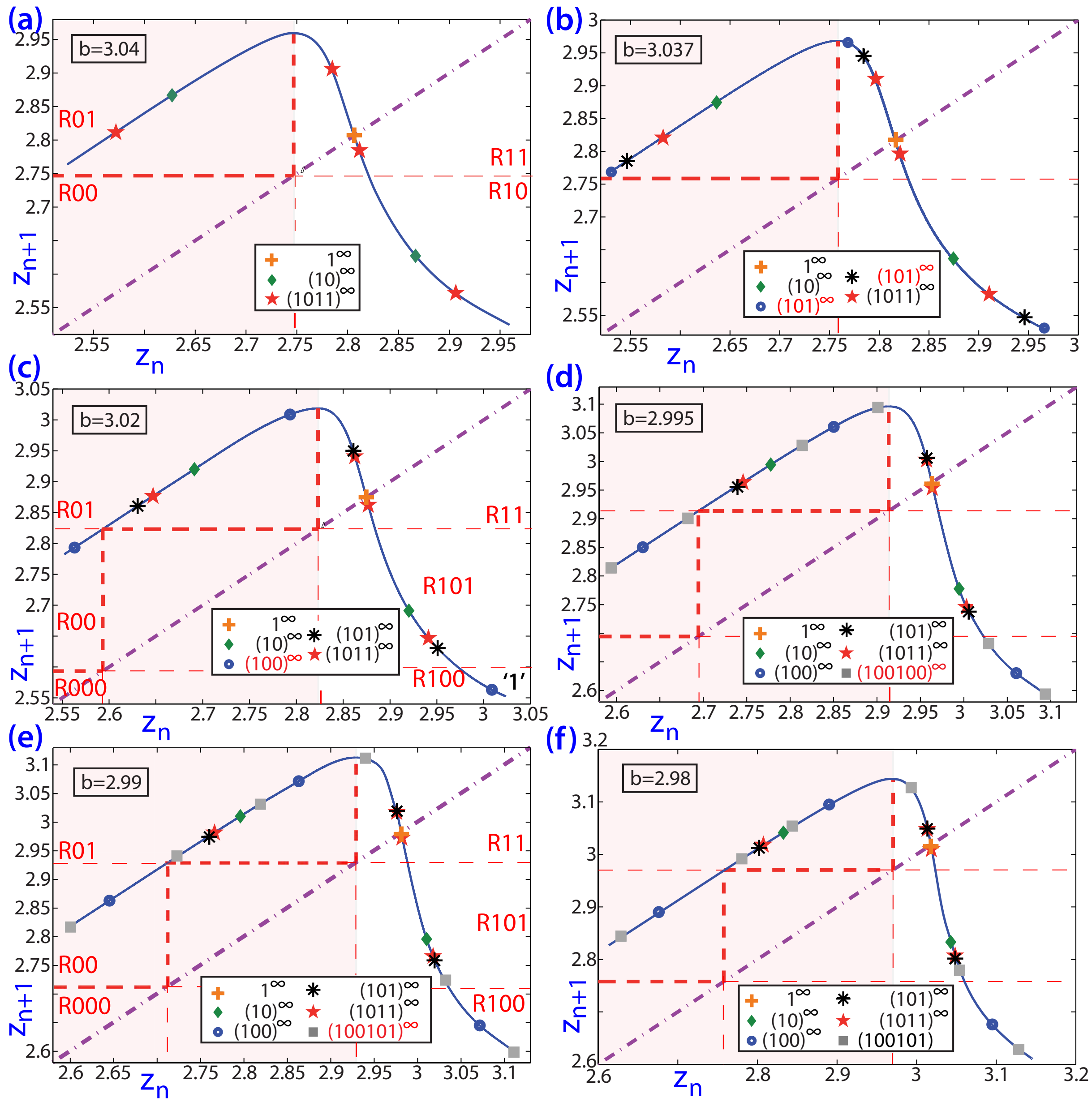

FIG. 4. First Return Map (using the Poincaré section $x = 0$, with $\dot{x} > 0$, and selecting the z component) of the chaotic invariant set (blue line) and of periodic orbits (different symbols) together with their symbolic sequences for different values of the parameters b and I: (a) $b = 3.04$; (b) $b = 3.037$; (c) $b = 3.02$; (d) $b = 2.995$; (e) $b = 2.99$; (f) $b = 2.98$, in the selected straight line $I(b) = (1 - 0.265b)/0.0691$ (see the dots in the thick yellow segment in Fig. 1 from right to left). The red lines determine the regions according to the behavior of their points when transformed by the map.

In addition to the FRM of the chaotic set, the FRMs of some existing low-period periodic orbits are represented in Figure 4 (with different symbols). Starting at $b = 3.04$, the kneading sequence of the existing chaotic attractor for this value begins with $(101)^6(01)^3 10\ldots$. If we look at ordination (4), we can see that this sequence is between $(10110)^\infty$ and $(101)^\infty$. As we have already mentioned, the orbit 0^∞ does not appear in the model, but the next five periodic orbits of (4) will be embedded in the chaotic attractor. We only draw the first three orbits (of lower period) so as not to add unnecessary complexity to the figure. The red dashed lines, and the regions delimited by them, serve as a reference to indicate how one point of the FRM (and its symbol) is transformed to generate the next one through the map. Thus, in panel (a) we have four regions defined by these lines. The points to the left of the maximum have a symbol "0" and the points to the right symbol "1". For the points that are at the top (regions R11 and R01), the next point will have "1" as a symbol; while, for the points that are at the bottom (region R10), the next point will have "0" as a symbol. Thus, the orange cross corresponding to the 1^∞ orbit is on the diagonal and therefore will remain fixed on the map. If we place ourselves in the green diamond at the bottom right (region R10), corresponding to the initial symbol ("1") of orbit $(10)^\infty$, the map will take us to the diamond in the upper left (region R01) with symbol "0". And this point will be transformed by the map into the original one, thus initiating a new cycle of the periodic orbit. Finally, if we start with the lower right red star (initial "1" of orbit $(1011)^\infty$), we go to the left star (with symbol "0"), from there it goes to the star just below the diagonal and, finally, before returning to the initial symbol, it becomes the upper star. Also, as we can see, in this case, the FRM of the chaotic set has no points in the lower left region (region R00, below the dashed horizontal line), so two consecutive "0"s cannot appear in the symbolic sequence of any orbit embedded in it. In contrast, two consecutive "1"s can appear since there are points in the upper right area (in fact the 1^∞ orbit is inside the chaotic attractor). The same observation can also be deduced from the ordering that we have defined since a sequence with two consecutive "0"s would have to start with 100, but this sequence would be greater, in the defined ordering, than that of the kneading sequence of the chaotic attractor for this b value. In fact $(101)^\infty \prec (100)^\infty$ and, as commented before, $(101)^\infty$ is not admissible, so neither of them is. In the following panels we will highlight in red the symbolic chains of those periodic orbits that appear for the first time or that have changed their symbolic chain with respect to the previous panel.

At $b = 3.037$, panel (b), the system has a stable attractor consisting of a stable bursting periodic orbit with 3 spikes. In fact, we can see that there are two different orbits (one stable, blue circles, and the other unstable, black asterisks) of period 3, both with symbolic sequence $(101)^\infty$. Later we will see in detail how these orbits have appeared, but what is evident is that the $(101)^\infty$ orbits are now admissible. In panel (c), $b = 3.02$, new regions delimited by new red dashed lines appear. The main novelty is that the FRM of the chaotic invariant set has points in the left region below the upper horizontal red dashed line (region R00). So now two consecutive ”0”s are already allowed. Those points come from the transformation of points in the new lower right region (region R100, with symbol 1). So, three consecutive ”0”s will remain a forbidden string in the symbolic sequence. If we study what has changed between panel (b) and (c), we can see that the last (upper) point of the stable periodic orbit has gone from the right side to the left side changing its symbol from “1” to “0”. At the same time, the lower left point has come down from the upper region. Therefore, this orbit now has the sequence $(100)^\infty$ (marked in red in panel (c)). At $b = 2.995$, panel (d), orbit $(100)^\infty$ has become unstable (being embedded in the chaotic saddle) and, now, the stable orbit is formed by two cycles of 3 spikes whose sequence is $(100100)^\infty$ which, formally, is the same as the previous one, but we note that the periodicity is 6. We see clearly a symbolic change at $b = 2.99$, where the last (upper) point of the orbit passes from the left to the right, thus changing to sequence $(100101)^\infty$ (marked in red in panel (e)) and opening a new different sequence. In the last panel (f), with $b = 2.98$, the attractor is again chaotic. Its kneading sequence begins with $(10010)^2 01011\ldots$. We observe that all the (unstable) periodic orbits that have been appearing for the previous values (and many others that we have not seen) have been incorporated into the chaotic set. But the next periodic orbit that appears in (4), $(10010)^\infty$, is not yet admissible (and of course also the three consecutive ”0”s chain that must be in R000 region). With this figure we observe that the new periodic orbits with new symbolic sequences appear within the stability windows. This is why the fact of calculating the chaotic invariant set in its entire region of existence (regardless of whether it is an attractor or not) is a key element to explain where and how these orbits appear. We will discuss in the following sections the infinite process that will allow the forbidden sequences to appear.

Specifically, we will see that the two processes that we have observed in the description of this figure (the appearance of two periodic orbits with the same sequence, one stable and one unstable, on the one hand, and the change of the last symbol of the sequence of a stable periodic orbit, on the other) are sufficient to generate the infinite sequences corresponding to the infinite periodic orbits that shape the dynamics of the system.

III. SYMBOLIC DYNAMICS AND BIFURCATIONS

A. Symbolic-flip and infinite cascades of period-doubling bifurcations

In the previous section, we have seen that between the values of $b = 3.04$ and $b = 2.98$ several orbits are created and, with them, different symbolic sequences. In Figure 5 we show the bifurcation diagram with the Poincaré section (PSS) of the z-variable plotted against the b-parameter along the selected line on the interval $b \in [2.97, 3.05]$, containing all the values discussed above. The attractor, chaotic or a stable periodic orbit, is represented in green; while UPOs (obtained by continuation techniques using AUTO[34,35] software) are represented in solid lines with different colors. The symbolic sequences of some families of periodic orbits are shown. In addition, the dashed black line shows the position of the maximum of the FRM of the chaotic invariant set delimiting two zones, with symbol “0” (down) and “1” (up), respectively. Thus, we can observe in a continuous way how and where the new sequences are generated.

The set of UPOs embedded in the chaotic invariant set forms its skeleton[1]. As observed in Figure 5, none of these families cross the maximum line of the FRM, so their symbolic sequences remain unchanged. Let us now detail what happens to the family of the (green) stable orbit $(101)^\infty$. Initially, at $b \approx 3.0382$, we can see how, of the three sections from the PSS of the family there are two in the upper region (right branch of the FRM, with symbol “1”) and one section in the lower region (left branch of the FRM, with symbol “0”). Specifically, the sections are visited starting from the top (symbol “1”), then the bottom (symbol “0”) and finally the central section (“1”). When b decreases in Figure 5, we observe how the central section approaches the maximum curve (dashed black curve) until it reaches a point, $b \approx 3.0338$, where the section of the periodic orbit crosses the line (see remarked red point on the figure), that is, the corresponding point reaches the maximum of the FRM. Later, it moves from the right to the left branch of the FRM and, therefore, it changes the corresponding symbol (from “1” to “0”). We denote this change *symbolic-flip* bifurcation. Note that this is a symbolic bifurcation, not a topological one. In other words, what changes is the symbolic sequence of the periodic orbit, not its stability or any other topological property. After that, approximately at $b = 2.998$, the family $(100)^\infty$ undergoes a period-doubling bifurcation and it becomes unstable. The new family of stable periodic orbits, $(100100)^\infty$, crosses the maximum line, experiencing a new symbolic-flip bifurcation, and becomes $(100101)^\infty$. A new period-doubling bifurcation makes this orbit unstable and creates the family $(100101100101)^\infty$,

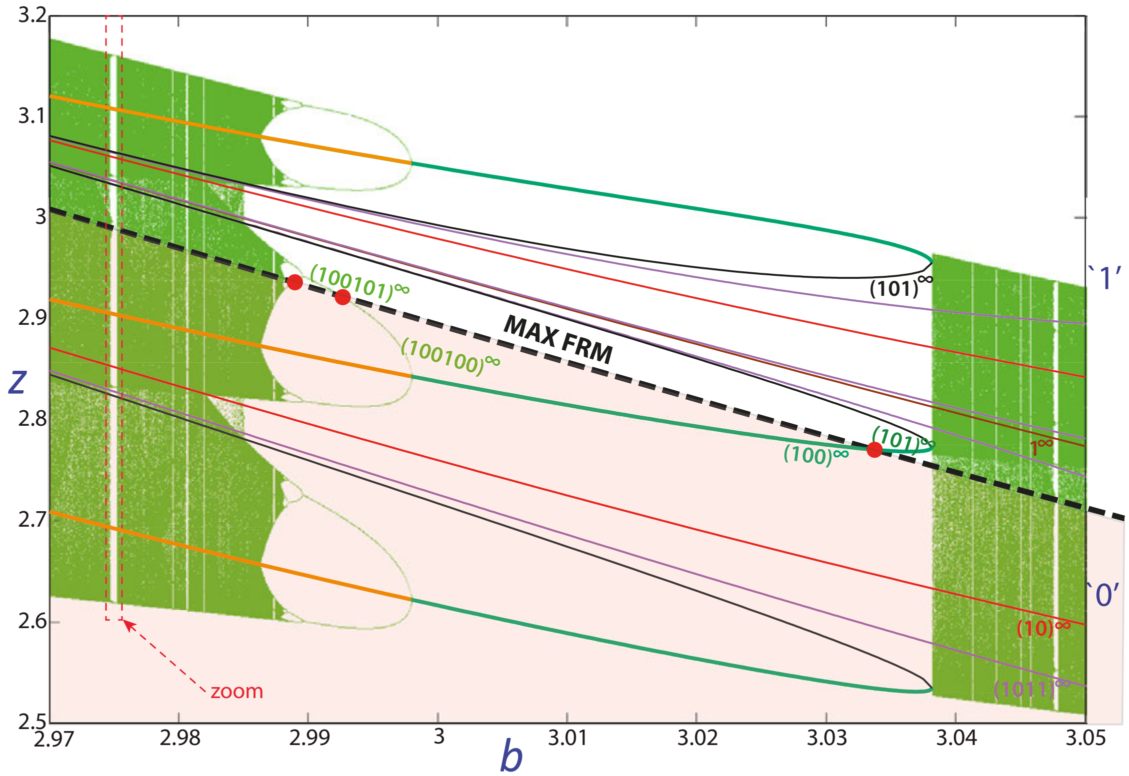

FIG. 5. Bifurcation diagram showing the PSS on the z-variable plotted against the b-parameter along the selected line $(I(b) = (1-0.265b)/0.0691)$. The corresponding attractors are shown in green, rest of continuous lines denote UPOs. Dashed black line identifies the position of the maximum on the FRM of the chaotic invariant set. When this line crosses the corresponding line of a stable periodic orbit, this periodic orbit experiences a symbolic-flip bifurcation (red points).

which will be transformed in another symbolic-flip bifurcation to $(100101100100)^{\infty}$. This process is repeated throughout an infinite cascade of period-doubling bifurcations until ending, at approximately $b = 2.9881$, in a chaotic attractor. This chaotic attractor has therefore incorporated all the UPOs that have been generated in this process.

The process just described is repeated identically in each stability window with $(S_f)^{\infty}$ the symbolic sequence of the basic stable periodic orbit of that window. Specifically, if $S_f = \Lambda s_f$ (s_f being the last symbol), after the first symbolic-flip bifurcation the new symbolic sequence will be $(S_s)^{\infty} = (\Lambda(1-s_f))^{\infty}$. And the infinite cascade of period-doubling and symbolic-flip bifurcations will occur:

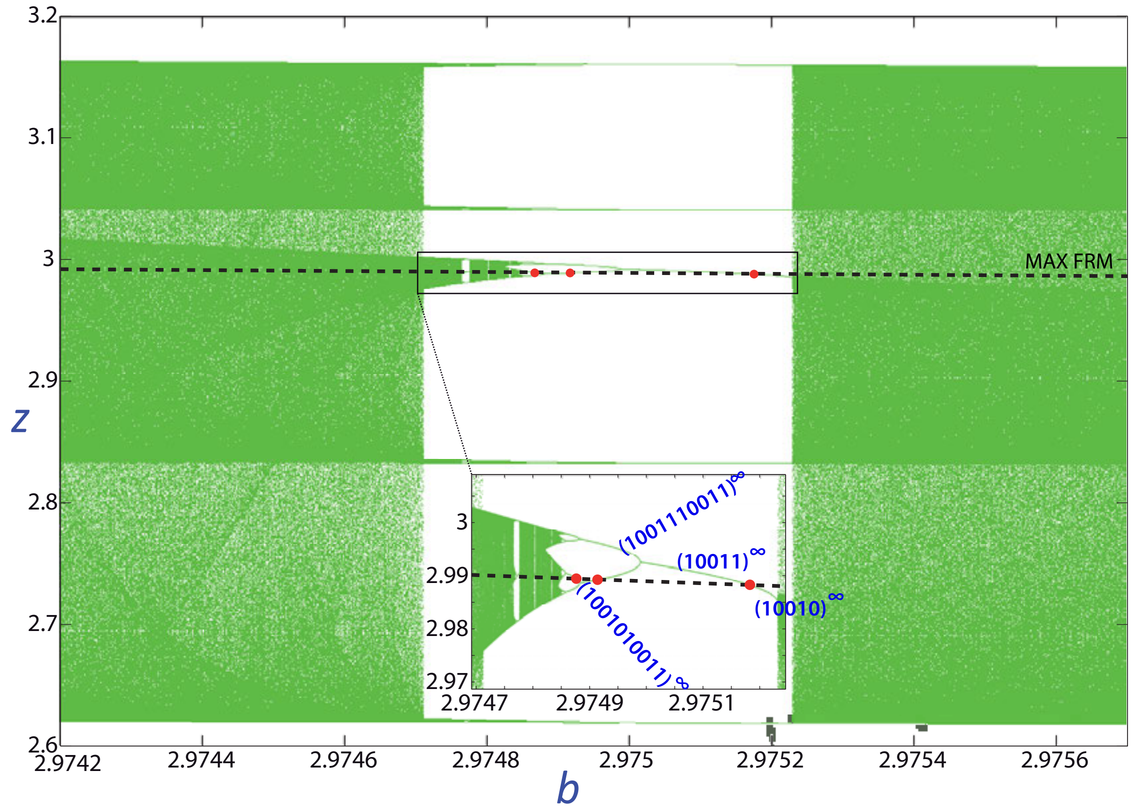

FIG. 6. Magnification of a narrow strip of Fig. 5 at a stability window of basic period 5. It shows the pattern of the infinite cascade of symbolic-flip (pointed in red) and period-doubling bifurcations.

$$(S_f)^\infty \xrightarrow{SF} (S_s)^\infty \xrightarrow{PD} (S_sS_s)^\infty \xrightarrow{SF} (S_sS_f)^\infty \xrightarrow{PD} (S_sS_fS_sS_f)^\infty \xrightarrow{SF} (S_sS_fS_sS_s)^\infty \xrightarrow{PD} \ldots \begin{array}{c}\text{chaotic}\\ \text{attractor}\end{array}$$

Note that, given the considered ordination and that the symbolic-flip bifurcation only changes the last symbol of the basic sequence that is repeated, this basic sequence must have an even number of "1"s, while the transformed basic sequence will have an odd number. Therefore, all the basic periodic orbits of a stability window will have a basic sequence with an even number of "1"s and it must undergo a period-doubling bifurcation to return to an even number of "1"s and to be able to cross a new symbolic-flip bifurcation. Figure 6 shows this general process in a magnification of the remarked small stability window on the left side of Figure 5. Here the basic sequence is 10010.

We have just seen how the infinite appearances of the symbolic-flip bifurcation on every (infi-

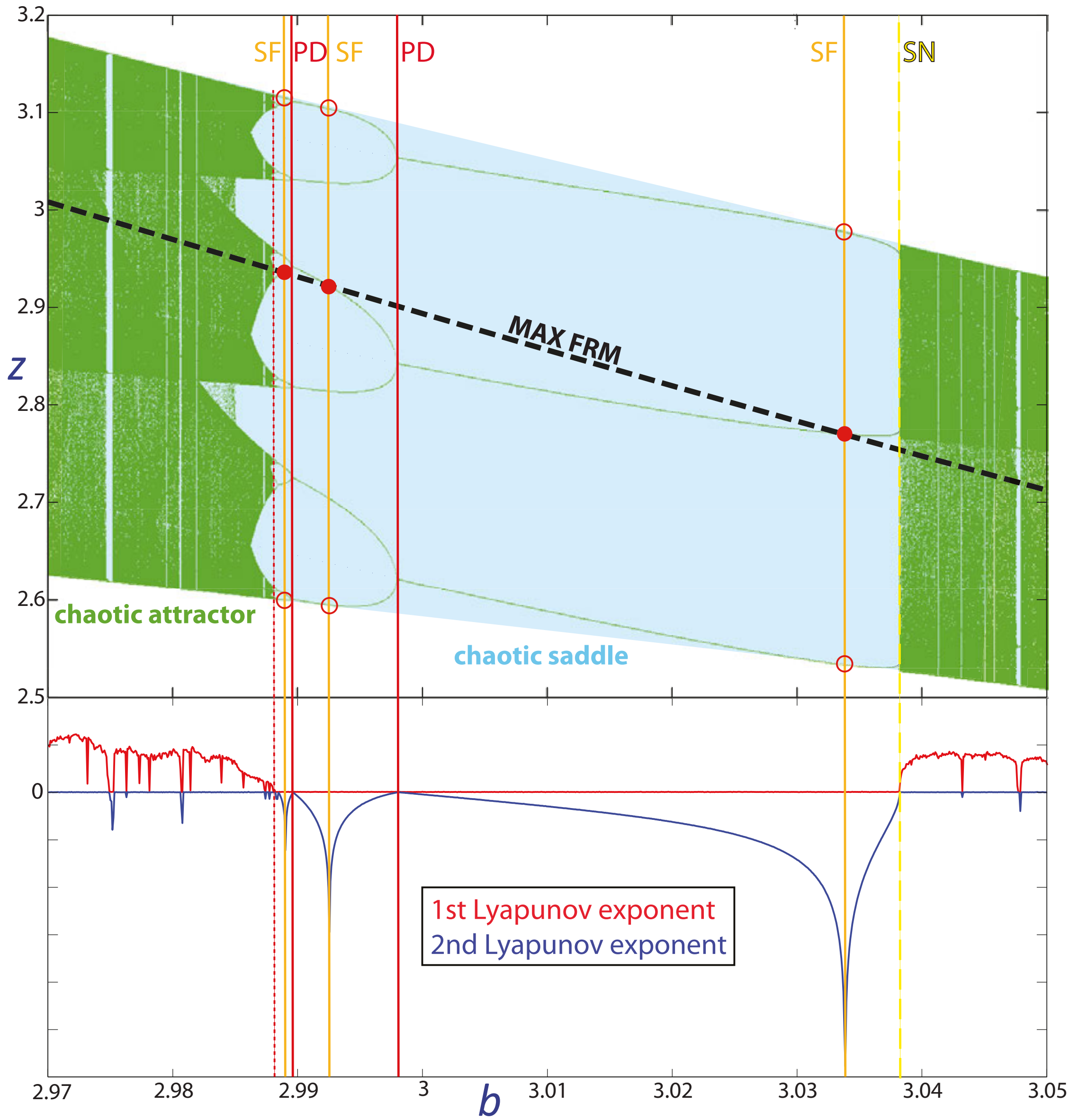

FIG. 7. Top: Bifurcation diagram showing the PSS on the z-variable plotted against the b-parameter along the 3-spikes basic stability window on the selected line ($I(b) = (1-0.265b)/0.0691$) and different bifurcations (Red: period-doubling (PD), Yellow: saddle-node bifurcation of limit cycles (SN), Orange: symbolic-flip bifurcation (SF)). Bottom: First and second Lyapunov exponents pointing out the different kinds of bifurcations.

nite) stability window that appears in a bifurcation diagram, open infinite symbolic sequences. In fact, we are going to see that this bifurcation is necessary to gradually generate the vast majority of periodic orbits that will end up forming the skeleton of the chaotic invariant set. Let us analyze in more detail some characteristics of the symbolic-flip bifurcation. As already mentioned, the bifurcation occurs when one of the points in the FRM of the periodic orbit reaches the maximum of the chaotic FRM. Thus, that section passes from one branch to another and, therefore, changes the corresponding symbol. When this happens, the next point in the FRM of this orbit is on the far right side of the FRM and the next one on the far left side. That is, the PSS of the periodic orbit touches both ends of the PSS of the invariant chaotic set. Besides, for a map, when a periodic orbit contains a critical point of the FRM, then this periodic orbit is said to be superstable (the tangent at that point is horizontal and therefore the derivative of the map is 0). In the continuous system (1) this situation is also marked by a minimum in the second Lyapunov exponent of the periodic orbit (see Figure 7). Moreover, at saddle-node and period-doubling bifurcations, the second Lyapunov exponent takes the value zero. Between two consecutive saddle-node and PD bifurcations the behavior of the system is regular (no chaotic) and, therefore, the second Lyapunov exponent is negative. It follows that between the two bifurcations there must be at least a minimum of this Lyapunov exponent. And therefore, there is a symbolic-flip bifurcation before each period-doubling, enabling this bifurcation to occur and to generate a new stable periodic orbit that makes the previous one unstable. All these circumstances can be observed in Figure 7. The fact that the second Lyapunov exponent of the periodic orbit in the continuous system marks the point at which its symbolic sequence changes will allow us, in Section IV, to continue the symbolic-flip bifurcation curves without the need to obtain the chaotic saddle throughout the phase space. On the other hand, this also reaffirms, as in the case of the determination of topological templates, that the symbolic study carried out makes both topological and dynamic sense.

Thus, we have seen that the symbolic-flip bifurcation is fundamental for the generation of the infinite periodic orbits that configure the dynamics of the system. However, this is not enough since the infinite cascade of symbolic-flip and period-doubling bifurcations ends on a chaotic attractor that cannot by itself change its symbolic sequence or generate new periodic orbits. An additional bifurcation is necessary that makes the chaotic set stop being an attractor and generates a new periodic orbit with a new sequence. This bifurcation is a saddle-node bifurcation of limit cycles (SN), which actually generates two new periodic orbits, one stable and the other one unstable. We will see below how the orbits that arise from this bifurcation appear as a limit of orbits that are previously generated accumulating in the fold.

B. Saddle-node bifurcation: a limit point

Let's continue with the 3-spikes basic stability window whose symbolic sequence is $(101)^\infty$ and we will demonstrate the following result.

Lemma 1 :

$$((101)^k0)^\infty \prec ((101)^k1)^\infty \prec ((101)^{k+1}0)^\infty \prec ... \prec (101)^\infty, \quad \forall k \geq 1.$$

Proof: Since $\rho((101)^k0) = +1$ (and so $\rho((101)^k1) = -1$), from (3) the first inequality is immediate. For the second inequality, we have to take into account that $((101)^k1)^\infty = (101)^k1101...$ and that $((101)^{k+1}0)^\infty = (101)^k1010....$ So, the leading common part is $(101)^k1$, $\rho((101)^k11) = +1$ and the second inequality is also satisfied. For the last inequality it is only necessary to observe that $(101)^\infty = (101)^{k+1}101(101)^\infty$. Then, the leading common part is $(101)^{k+1}$ with $\rho((101)^{k+1}0) = +1$. $\boxtimes$

On the other hand, it is easy to see that when k tends to infinity the last symbolic sequence is the limit of all other sequences. The previous result shows that, as b decreases in our parametric line, the chaotic invariant set incorporates longer and more frequent substrings of the type $(101)^k$. Until, finally, the chaotic attractor becomes a chaotic saddle and a stable periodic orbit (and also an unstable one) with symbolic sequence $(101)^\infty$ appears. This occurs at a saddle-node bifurcation. This process can be observed in Figure 8, where we show the time series of the basic bursting orbits with 2 and 3 spikes and of several chaotic attractors as b approaches the limit value where the saddle-node bifurcation takes place and the periodic orbit $(101)^\infty$ appears. In the figure we can see how, for the first considered values of b ($b = 3.06$ and 3.05), pattern 101 appears scarcely, whereas pattern 10 is much more frequent. As b decreases, pattern 101 repeats more frequently and the orbit resembles more to the basic orbit with 3 spikes. In fact, at the last considered value of b, it is necessary to extend the representation time to see that the dynamics are not yet periodic. This fact can also be appreciated from the kneading sequence of the corresponding chaotic attractor. Actually, this result can be generalized for any stability window.

Theorem 1 : *Let $(\Lambda s_f)^\infty$ be the symbolic sequence of the basic periodic orbit of a stability window generated at a saddle-node bifurcation. Then it is fulfilled*

$$((\Lambda s_f)^k0)^\infty \prec ((\Lambda s_f)^k1)^\infty \prec ((\Lambda s_f)^{k+1}0)^\infty \prec ... \prec (\Lambda s_f)^\infty, \quad \forall k \geq 1.$$

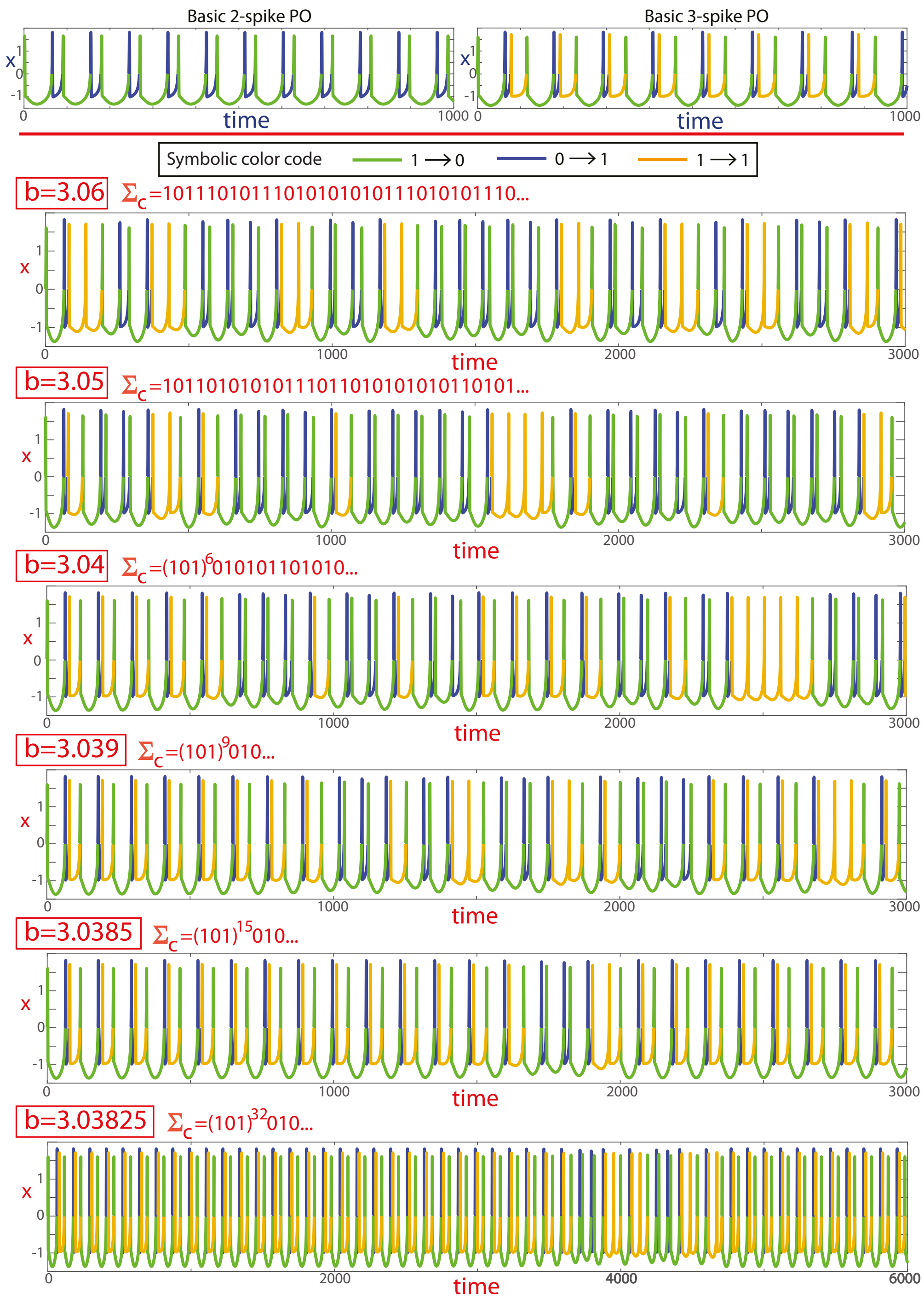

FIG. 8. Time series of the basic stable bursting periodic orbits with 2 and 3 spikes and of the chaotic attractors for different values of b approaching the value where the saddle-node bifurcation occurs when the basic orbit with 3 spikes appears, approximately at $b = 3.0382$. The color code represents the transformation of each section of the orbit in the FRM. Σ_c is the kneading sequence of the corresponding chaotic attractor.

Proof: The proof is similar to the previous Lemma 1 considering that Λs_f has an even number of

"1" and it begins with 10 due to the canonical representation we have chosen in Section II. Then, $\rho((\Lambda s_f)^k 0) = +1$ and, using (3), the first inequality is immediate. For the second inequality, we have $((\Lambda s_f)^k 1)^\infty = (\Lambda s_f)^k 110...$ and $((\Lambda s_f)^{k+1} 0)^\infty = (\Lambda s_f)^k 10...$ So, the leading common part is $(\Lambda s_f)^k 1$, $\rho((\Lambda s_f)^k 11) = +1$ and the second inequality is also satisfied. For the last inequality it is only necessary to observe that $(\Lambda s_f)^\infty = (\Lambda s_f)^{k+1} 10...$ Now, the leading common part is $(\Lambda s_f)^{k+1}$ and $\rho((\Lambda s_f)^{k+1} 0) = +1$, what gives the desired result. ⊠

Obviously, between these inequalities we could introduce other infinite successions of symbolic sequences, corresponding to other infinite periodic orbits. All of them will converge to the symbolic sequence of the basic periodic orbit of the corresponding stability window.

C. Self-similarity

As we have seen in the previous subsections, the same process occurs in each stability window. In a saddle-node bifurcation, originated as a limit of different families of previous periodic orbits, two periodic orbits are generated (one stable and the other one unstable). The stable orbit undergoes an infinite cascade of symbolic-flip and period-doubling bifurcations until the dynamics of the system become chaotic. This situation, which is reproduced in the infinite stability windows, generates a certain level of self-similarity[36]. However, that self-similarity is much deeper, as it is not limited to the process of transforming the families of periodic orbits within each separate window. But it also affects how different windows appear along a certain segment. To understand better this phenomenon we will make use of the *-composition law[36]. Let Λ be a finite symbolic sequence and $\Sigma = s_1 s_2 ...$ a (finite or infinite) sequence, then $\Lambda * \Sigma$ is defined as

$$\Lambda * \Sigma = (\Lambda * s_1)(\Lambda * s_2)..., \quad \text{where } (\Lambda * s_i) = \begin{cases} \Lambda 0 \text{ if } \rho(\Lambda s_i) = +1, \\ \Lambda 1 \text{ if } \rho(\Lambda s_i) = -1. \end{cases} \tag{5}$$

Note that by construction $\rho(\Lambda * s) = \rho(s)$ and, so, $\rho(\Lambda * (s_1 s_2 ... s_k)) = \rho(s_1 s_2 ... s_k)$. Therefore,

$$\Sigma_1 \prec \Sigma_2 \Leftrightarrow \Lambda * \Sigma_1 \prec \Lambda * \Sigma_2.$$

Then, if we take a symbolic dynamics interval $I_{\text{sym}} = [\Sigma_1, \Sigma_2]_{\text{sym}}$ with $\Sigma_1 \prec \Sigma_2$ and a finite sequence Λ, the interval $I^{\Lambda}_{\text{sym}} = [\Lambda * \Sigma_1, \Lambda * \Sigma_2]_{\text{sym}}$ contains exactly the same bifurcations as I_{sym} (and in the same order), with the only difference that the bifurcations and changes are applied to the orbit $\Lambda * \Sigma_k$ instead of Σ_k, where $\Sigma_k \in I_{\text{sym}}$[36]. Since Λ can be any finite sequence and for each of them we obtain a symbolic interval I^{Λ}_{sym} with the same bifurcations, any symbolic interval I_{sym} has infinite

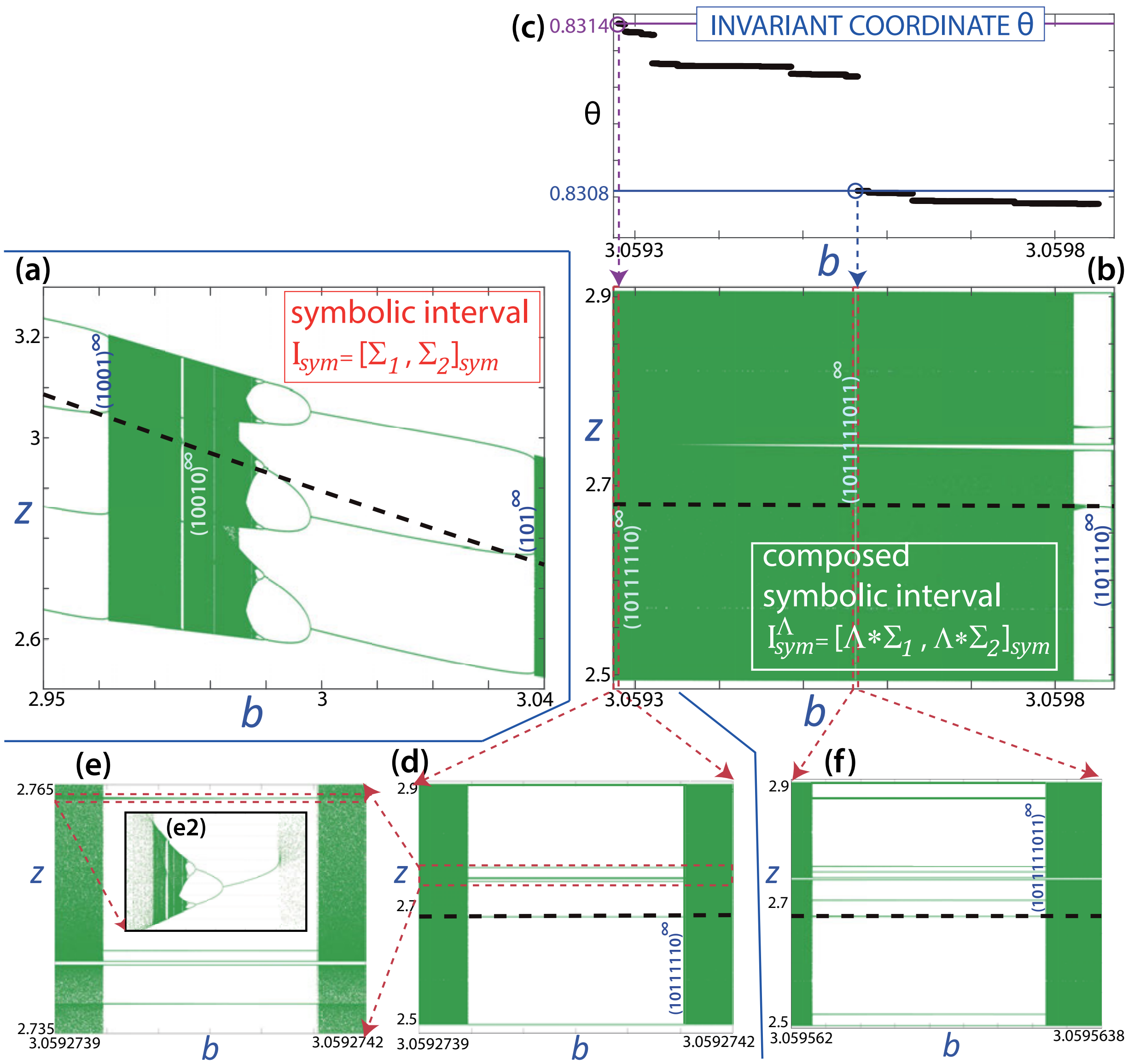

FIG. 9. Bifurcation diagrams for (a) $I_{\text{sym}} = [\Sigma_1, \Sigma_2]_{\text{sym}} = [(101)^\infty, (1001)^\infty]_{\text{sym}}$ and (b) $I^{\Lambda}_{\text{sym}} = [\Lambda * \Sigma_1, \Lambda * \Sigma_2]_{\text{sym}} = [(101110)^\infty, (10111110)^\infty]_{\text{sym}}$ with $\Lambda = 1$. It can be seen that the correspondence between the bifurcations of both intervals is not visually detected (see explanation in the text). (c) Invariant coordinate θ calculated for the symbolic sequences inside I^{Λ}_{sym} and used for detecting stability windows for $\Lambda * (1001)^\infty = (10111110)^\infty$ and $\Lambda * (10010)^\infty = (1011111011)^\infty$ (represented on magnifications (d) and (f), respectively). Two more successive enlargements (plots (e) and (e2)) are necessary to begin to observe this correspondence.

replicas of itself. It should be noted that self-similarity refers to the bifurcations experienced by the families of the orbits, not to the length of the different stability windows. In fact, it is visually very difficult to observe this level of self-similarity because the size of the corresponding stability windows between one symbolic interval and another can be very different.

We illustrate this phenomenon with an example. If we take $I_{\text{sym}} = [(101)^\infty, (1001)^\infty]_{\text{sym}}$ and $\Lambda = 1$, then (see (5)) $\Lambda * (101)^\infty = ((1*1)(1*0)(1*1))^\infty = (101110)^\infty$ and $\Lambda * (1001)^\infty = ((1*1)(1*0)(1*0)(1*1))^\infty = (10111110)^\infty$, therefore $I^\Lambda_{\text{sym}} = [(101110)^\infty, (10111110)^\infty]_{\text{sym}}$. Figure 9 (a) and (b) show the bifurcation diagrams on both intervals that englobe I_{sym} and I^Λ_{sym}, respectively, within the line selected in Figure 1. Visually there is no similarity at first sight. In fact, it is necessary to carry out several successive magnifications (plots (d), (e) and (e2)) to observe what happens in the window that contains one of the ends of I^Λ_{sym}. The same goes for interior stability windows. Also, the window sizes in I^Λ_{sym} are so small that you must use the *invariant coordinate*[26] of the searched symbolic sequence to locate them.

Given an infinite sequence $\Sigma = s_0 s_1 s_2 \ldots$, its *invariant coordinate* $\theta(\Sigma)$ is defined as

$$\theta(\Sigma) = \sum_{i=0}^{\infty} \frac{t_i}{2^{i+1}}, \qquad \text{with } t_0 = s_0 \text{ and } t_i = \begin{cases} s_i & \text{if } \rho(s_0 \ldots s_{i-1}) = +1, \\ 1 - s_i & \text{if } \rho(s_0 \ldots s_{i-1}) = -1, \end{cases} \quad \forall i \geq 1. \tag{6}$$

Then, $\theta(\Sigma) \in [0,1]$ and $\Sigma \prec \Sigma' \Leftrightarrow \theta(\Sigma) < \theta(\Sigma')$. Using this definition, we can obtain the value of θ for the two ends of the interval, $\theta((101110)^\infty) = 52/63 \simeq 0.82539682539\ldots$ and $\theta((10111110)^\infty) = 212/255 \simeq 0.831372549\ldots$ (do not forget that the given ratios correspond to the infinite sequences), and for any interior orbit, for example $\theta((1011111011)^\infty) = 850/1023 \simeq 0.830889540\ldots$ (note that $1 * (10010) = 1011111011$). Thus, to locate the symbolic dynamics interval I^Λ_{sym}, we calculate θ from the sequences obtained with the points of the bifurcation diagrams of a wide interval and, using the fact that θ is a monotonically increasing function, we can detect the value of θ of the periodic orbits we are interested on and, with it, the value of b where its stability window is located. This simple approach has allowed us to detect where a particular periodic orbit appears depending on the parameter b and later to locate the corresponding periodic window independently its size. Plot (c) at the top of the Figure 9 shows the value of θ in the region that interests us. The values of θ for orbits $(10111110)^\infty$ and $(1011111011)^\infty$ are marked with a purple and blue horizontal line, respectively. The corresponding vertical dashed line indicates the approximate value of the parameter b at which the orbit is located with these given sequences. Note that the jumps shown in the θ graph occur only at symbolic-flip bifurcations since period-doubling bifurcations do not change the sequence of the created orbit and the saddle node appears as a limit. The regions shown enlarged in plots (d) and (f) have been located with this technique. It

PLEASE CITE THIS ARTICLE AS DOI: 10.1063/5.0043302

is important to remark the difficulty of detecting and analyzing this level of self-similarity without using the symbolic dynamics of the system, and the crucial help of using the invariant coordinate as a numerical tool to locate particular periodic orbits.

IV. GLOBAL ANALYSIS

In the previous section we have studied the different bifurcations that originate and modify the periodic orbits of the system along a particular parametric line $I(b) = (1-0.265b)/0.0691$, but we have not studied the influence of these bifurcations in the position of the periodic orbits in the chaotic attractors in the parametric plane (b, I), and the global structure along the complete line. And moreover, it remains an important question, what happens when we move the small parameter ε?

A. Spike-adding and open sequences

We have described in detail what happens before, during and after the stability window whose basic bursting orbit has three spikes (Figures 5, 7 and 8). Among other things, we have seen that the originated stable periodic orbit whose symbolic sequence is $(101)^\infty$ undergoes a symbolic-flip bifurcation where its sequence changes to $(100)^\infty$. At that bifurcation the FRM of the chaotic invariant set (at that time a saddle invariant set) begins to have a region on the left part of the figure containing those points of the branch on the left (symbol “0”) that are transformed into other points also on the branch on the left. This opens the possibility of sequences with two consecutive “0”s that, for higher values of b, were forbidden (see Figures 4 and 5).

In Figure 1 you can see how the selected line crosses the different chaotic stripes and, after each one, the new stability window has a basic orbit with one spike more than in the previous window. A chaotic spike-adding has taken place[10]. As occurred in the previous stripe to the appearance of orbit $(101)^\infty$, families of orbits will be generated along each chaotic stripe, which will eventually converge to orbit $(10^n1)^\infty$, which will undergo a symbolic-flip bifurcation where it will change its symbolic sequence to $(10^{n+1})^\infty$ opening the possibility of new sequences with $n+1$ consecutive “0”s that will be generated along the next chaotic stripe. Therefore, as we move to the left the value of parameter b inwards on the selected line, more consecutive zeros are allowed in the symbolic sequence of the orbit. In Figure 10 we present a 3D plot by combining a bifurcation diagram with

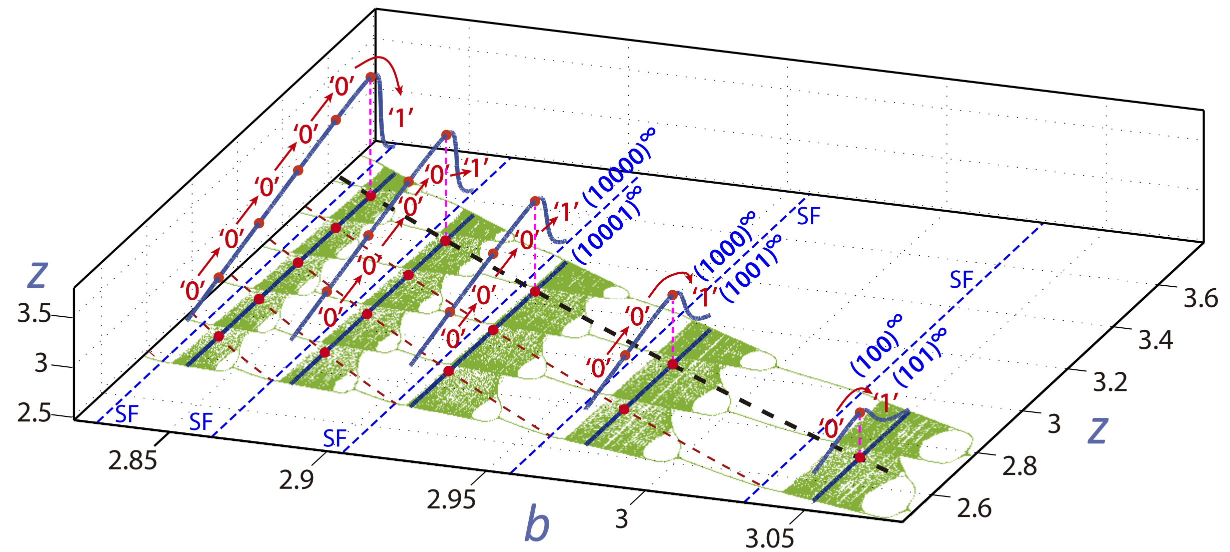

FIG. 10. Bifurcation diagram showing the PSS z-variable plotted against the b-parameter along the selected line crossing five chaotic layers. The third dimension presents several FRMs, red points delimit the boundaries between regions with different numbers of zeros in the symbolic sequence of the orbit (see the text).

the PSS z-variable plotted against the b-parameter in a portion of the selected line (crossing the first five chaotic stripes), and the third dimension showing several FRMs. As we have already seen, as b decreases, new periodic orbits (with new symbolic sequences) are generated. These periodic orbits occupy new spaces that thicken the chaotic set when they are incorporated into it. This thickening can also be seen in the PSS shown in the figure.

The FRMs exhibit red points delimiting the boundaries between regions with different behavior according to the symbolic sequence of the orbit. This means that, if in the FRM there is only one red point (at the maxima), then only one consecutive “0” is allowed in the symbolic sequence as the FRM is not big enough to have opened the possibility of two zeros. In case of two red points we have in the FRM the option of two consecutive zeros, and so on. Each spike-adding bifurcation increases the maximum length of allowed chains of consecutive “0”s by one. As for the basic periodic orbit with two spikes the symbol 0 is allowed, but not the chain 00, in the region with basic periodic orbit with k spikes, the maximum number of consecutive “0”s is $k-1$. The dashed red lines on the floor plot mark the regions in the PSS with a different number of consecutive future “0”s. The dashed blue lines mark the values of b where a symbolic-flip bifurcation transforms sequence $(10^n1)^\infty$ into sequence $(10^{n+1})^\infty$. Note that, at the b value where the dashed black line crosses the bifurcation diagram for the basic periodic orbit with $n+2$ spikes ($n \geq 1$), that orbit experiments a symbolic-flip bifurcation (SF) and this is the value where the dashed red curves are originated. We just show the first SF bifurcations on some periodic windows. This process is repeated as many times as there are spike-addings. So, if orbit $(10^k)^\infty$ is generated but not $(10^{k+1})^\infty$, then no sequence $\Sigma \succ (10^{k+1})^\infty$ will be allowed. Therefore, the process of completing all the possible symbolic sequences is related with the spike-adding phenomena and how many there are.

B. Position of periodic orbits

The different existing periodic orbits, when unstable, are incorporated into the skeleton of the chaotic invariant set. Next, we will analyze how the point in the parametric space where each periodic orbit appears determines the position that the periodic orbit will occupy physically inside the chaotic invariant set.

In Figure 11 we show some of the UPOs used in the template analysis of three different chaotic attractors inside the selected line $I(b) = (1-0.265b)/0.0691$ (for $b = 2.625$, 2.69 and 3.05). On this plot we observe that the chaotic attractors for $b = 2.625$ and 3.05 are more similar between them than for $b = 2.69$. The cases $b = 2.625$ and 3.05 have their UPOs all along the chaotic attractor, but on the case $b = 2.69$ the low multiplicity UPOs are located only on one side. The next figures will try to explain this fact.

Continuing with the previously selected line, Figure 12 shows at the bottom (plot (c)) the PSS of the attractor (in a fine green line) and of the periodic orbits (thick colored lines) up to multiplicity 4. As we can see, when a periodic orbit is created, it appears in the spatial region determined by the chaotic set (at that time of saddle type) existing for those parameter values. As we saw in previous subsection, the size of the FRM (originated by the size of the chaotic set) increases as b decreases in the studied line (but close to the left end, as we will explain later). On the other hand, we have observed in Subsection III A that unstable orbits do not change their symbolic sequences (see Figure 5). Thus, the unstable orbits in our figures do not cross any of the curves that define the different regions that delimit the number of consecutive zeros (see Figure 10).

If we look closely at Figure 10, we can see how these curves delimiting the number of consecutive zeros divide the PSS of the stability window in regions, one per each spike-adding phenomenon. Each of these regions roughly correlates with each of the lobes generated by each

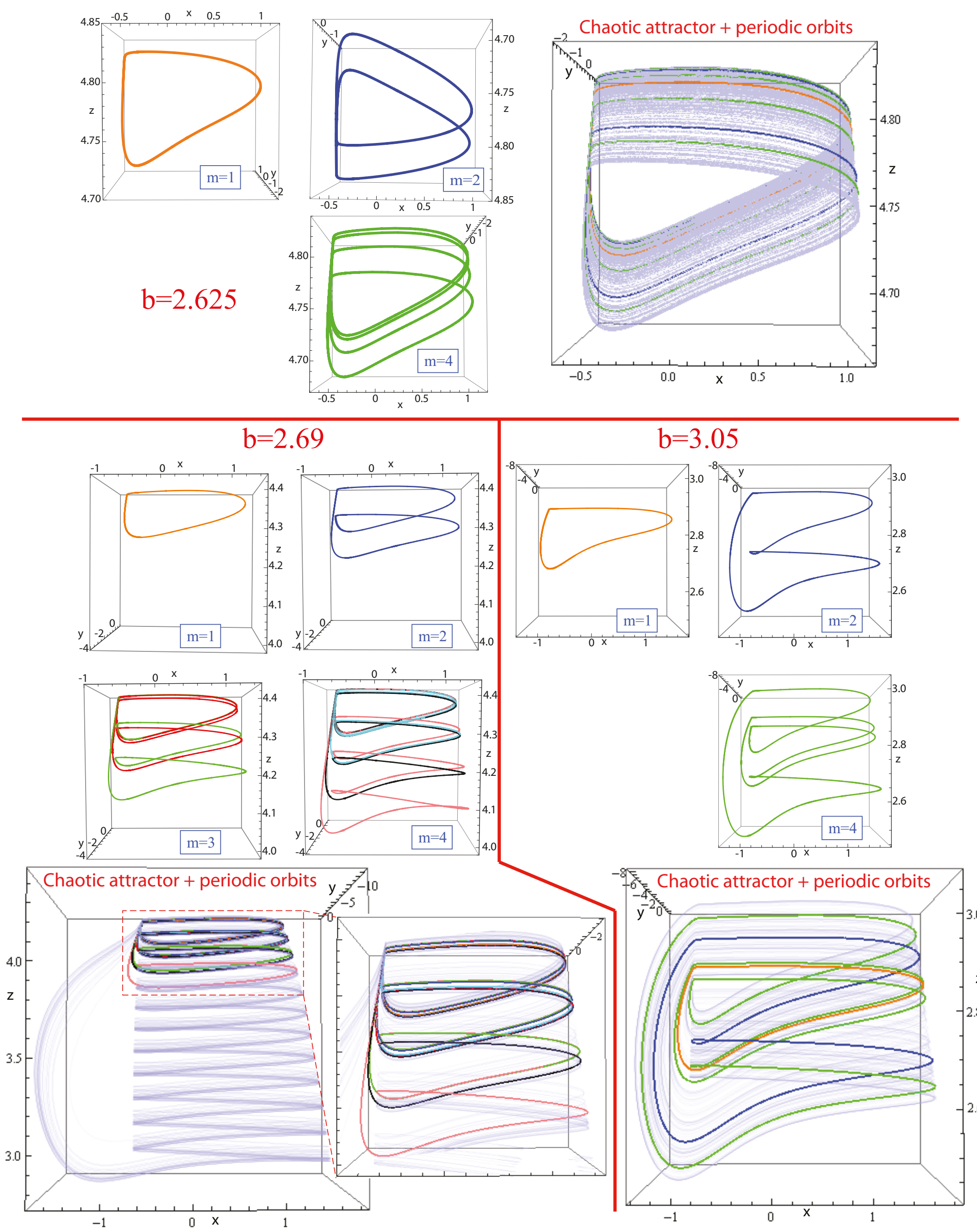

FIG. 11. All UPOs up multiplicity four for three selected chaotic attractors ($b = 2.625$, 2.69 and 3.05 with $I(b) = (1 - 0.265b)/0.0691$). Plotting these orbits over the chaotic attractor on faint color, we can see that not only the attractor, but also the periodic orbits, change with the increment of the parameter b and how they are located spatially on the attractor on specific regions.

number of spikes of the basic stable orbit. In addition, these regions are ordered in the same order as they appear. That is, the family of orbits that has been generated in a set of parame-

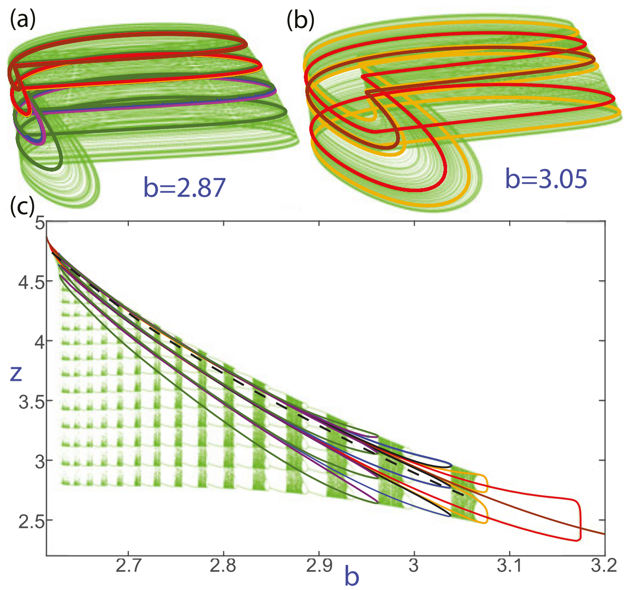

FIG. 12. (a) and (b): chaotic attractor (thin green line) for two different values of b in the selected line $I(b) = (1-0.265b)/0.0691$. The UPOs up to multiplicity 4 foliated to the chaotic attractor are shown with thick lines of different colors. (c): bifurcation diagram showing the PSS on the z-variable plotted against the b-parameter along the selected line. The same color code has been used for all the pictures.

ters in which the PSS of the chaotic set has been divided into n regions will remain located in those n regions throughout its entire existence. We can see this circumstance in Figure 12, where the curves corresponding to families with lower symbolic sequence (and so, they appear earlier) occupy only upper lobes of the PSS. Looking at the chaotic set, the periodic orbits that were generated previously cannot traverse physically to the part with lower values of z, corresponding to higher symbolic sequences (see the two chaotic attractors in the top of the figure).

In addition, we can observe that those pairs of periodic orbits that appear in the same saddle-node bifurcation, although initially they are indistinguishable, when b decreases both orbits are distanced and the initially stable orbit (which is the one that changes its symbolic sequence) goes through more extreme values of z. This reinforces the fact that the symbolic sequence of the orbit conditions the regions of the chaotic invariant set that an orbit can visit.

The FRM and the bifurcation diagram have provided us information about the symbolic sequences that are appearing successively. Now the question is, taking one chaotic invariant set in the fast-slow system (the HR model in our case), how the loops around the fast manifold generate the route in the topological template and the possible symbolic sequences. In Figure 13 we show,

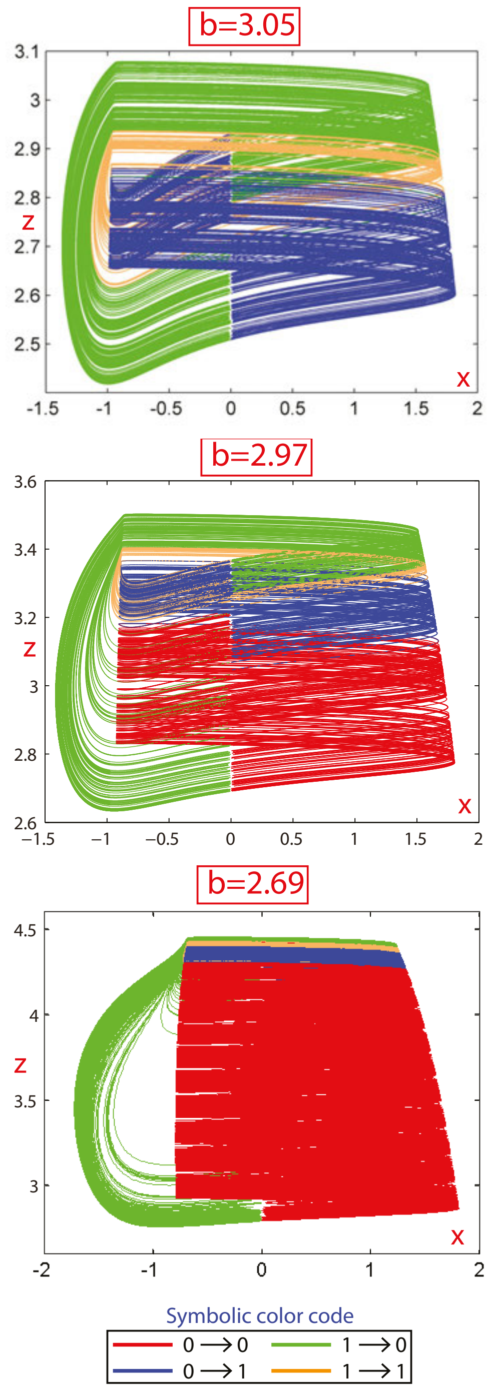

FIG. 13. Chaotic attractor projections for different parameter values. Different colors indicate different evolution on the symbolic sequence for the chaotic orbit (see the text for more details). Note how the different symbolic chains are located in different regions of the chaotic attractor.

for three parameter values on the selected line, the chaotic attractor, and we use different colors to show how the different spikes are connected with the symbolic sequence. For the case $b = 3.05$, the chaotic attractor is situated close to the band corresponding to 2-bursting (that is, a bursting orbit with two spikes in the active regime). The way the new spikes around the fast manifold are located corresponds with the symbolic sequence. We have used a color code to show this process. *Blue* color is related with a loop that goes from a symbolic value 0 to 1, *green* from 1 to 0, *brown* from 1 to 1 and *red* from 0 to 0. Note that this chaotic attractor has forbidden the chain 0 to 0, and so the red color is not present. In the case $b = 2.97$, the chaotic attractor is located close to the band corresponding to 3-bursting, and now the basic orbit is a 3-spike bursting orbit. The situation is similar as before, but what is new is the existence of a new sequence, 0 to 0 (*red* color). In fact the top part of the attractor is quite similar to the one as the case $b = 3.05$, and what is added is the red part with the new opened symbolic sequence 00. If we go far away in the process of spike-adding, for instance $b = 2.69$, the chaotic attractor is situated close to the band corresponding to 12-bursting. The process now is quite similar to the one observed before in case $b = 2.97$ with a 3-bursting. And also, the top part is again quite similar to the one as the case $b = 3.05$ (the green, brown and blue parts), what is added is a long red part that adds all the new opened symbolic sequences (allowed up to 11 consecutive zeros). This process is the same for all the chaotic attractors along the spike-adding process. That is, as it is shown in Figure 12, the UPOs are located in regions depending on when they appear and the new regions are related with extra sequences with more “0”s located on one extreme of the chaotic invariant set.

C. Three-parameter analysis

We have studied in detail the different bifurcations that originate and modify the periodic orbits of the system along the parametric line $I(b) = (1 - 0.265b)/0.0691$ for $\varepsilon = 0.01$. Now, we are going to study these bifurcations, leaving the three considered parameters (b, I and ε) free.

Taking into account that the second Lyapunov exponent reaches a minimum at each symbolic-flip bifurcation and using the continuation software AUTO, we have been able to locate the main bifurcations involved in the processes described above. Figure 14 shows the curves of these bifurcations, on the biparametric spike-counting sweep plate, in an area of the (b, I) plane around the interval studied in sections III A and III B. We can see how the period-doubling (red), saddle-node (dashed yellow) and symbolic-flip (orange) bifurcations curves are born at the black curve of homoclinic bifurcation. In fact, they are born at codimension-two points (inclination-flip and orbit-flip homoclinic bifurcations[37]) located on the homoclinic bifurcation curve, but a detailed

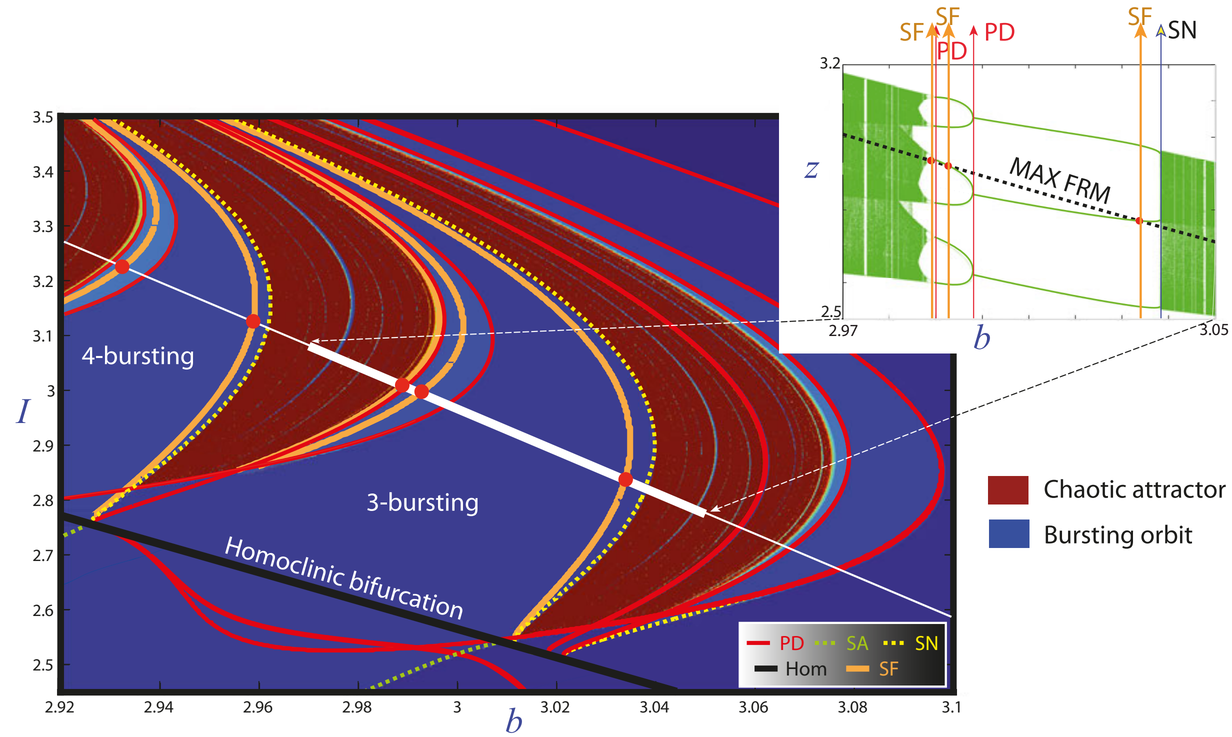

FIG. 14. (b, I)-parametric spike-counting sweep of HR model for a region centered on the interval analyzed in Figure 5. Several bifurcation lines of limit cycles (Black: homoclinic bifurcation, Red: period-doubling (PD), Yellow: saddle-node bifurcation (SN), Green: spike-adding area (SA)) are overlapping. Orange lines correspond with symbolic-flip bifurcations (SF). They exist between two consecutive PD bifurcations, and between SN and the first PD bifurcation on each pencil of bifurcations. The bifurcation diagram of the interval centered in the stability window of the basic 3-spike periodic orbit that has been previously studied in detail in Figure 5 is shown in the upper right corner.

study is far of the goal of this article and more details can be seen on references[9,11,12]. The bifurcation curves on the upper part of the homoclinic curve forms the chaotic bands detected in Figure 1. The intersections of these curves with the segment $I(b) = (1 - 0.265b)/0.0691$ selected in the previous sections give us the bifurcation points previously analyzed. The bifurcation diagram in the upper right corner is the same as in Figure 5, shown here to connect the previous uniparametric analysis with the current biparametric one.

If we expand the study region, we can see in Figure 15 how more stability regions appear on the left, separated by chaotic stripes. They are the successive spike-adding phenomena[9,11,12] previously discussed and, in all of them, the same processes occur as in the one we have already

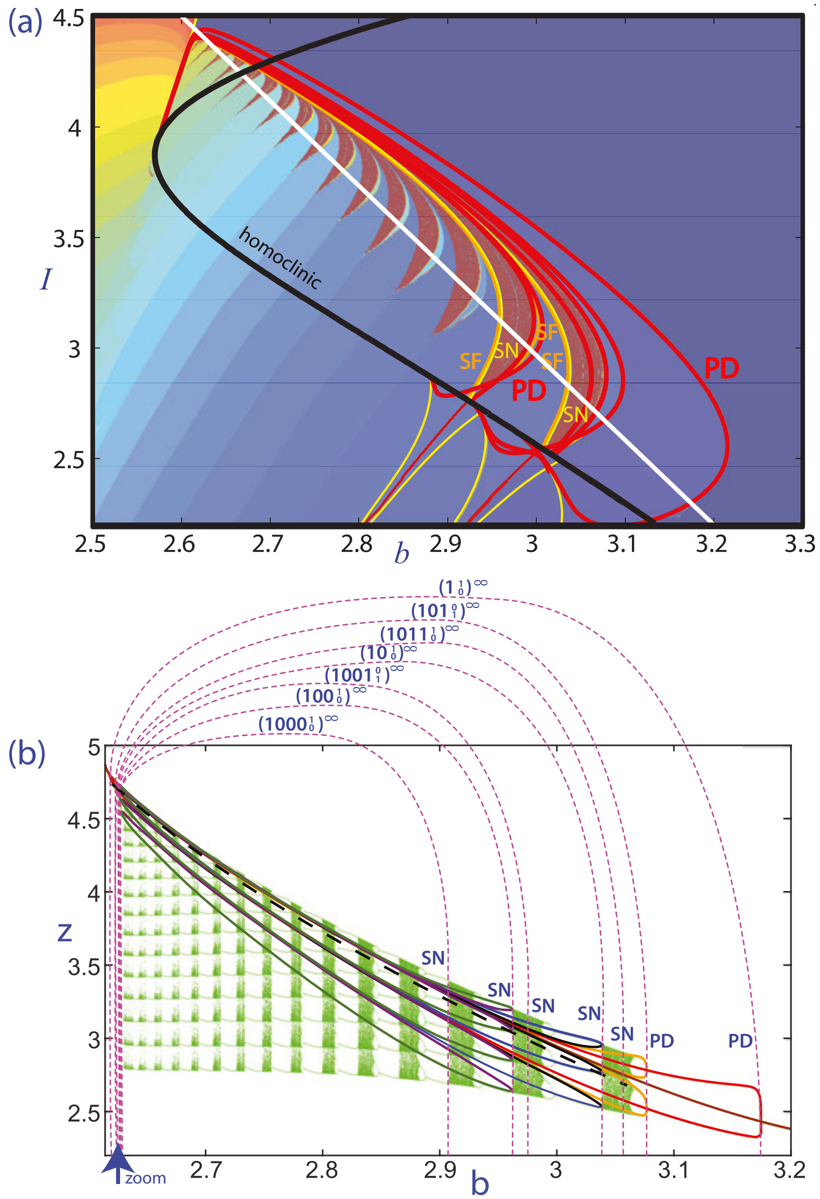

FIG. 15. (a): (b, I)-parametric spike-counting sweep of HR model for a region containing all the chaotic bursting (dark red) strips for $\varepsilon = 0.01$. (b): Bifurcation diagram along the selected (white) line with dashed pink curves delimiting the intervals where each periodic orbit, with multiplicity lower or equal to 5, exists.

described. The chaotic stripes stick to each other at the top and form a kind of onion layer structure that closes on the left side. That is, in the bursting region above the homoclinic bifurcation curve, as b decreases, there are more and more periodic orbits, which are added to the chaotic structure. However, at some point, by an inverse process, if b continues to decrease, the orbits disappear. At the bottom of Figure 15 we show this situation on the line $I(b) = (1 - 0.265b)/0.0691$. The pink dashed curves show the values of b at which the bifurcation that generates (or destroys) the periodic orbit occurs. The symbolic sequence on each curve is the one that corresponds to the orbit generated at the respective bifurcation. The last symbol shows two values because the corresponding stable orbit will soon undergo a symbolic-flip bifurcation that will change that symbol from the top to the bottom value. Therefore, in the selected line there are first period-doubling cascades and later period-halving cascades resulting in complete period-doubling cascades[38] in the sense that all period-doubling cascades are paired with period-halving cascades on the left part of the parameter plane. In fact this phenomena is completely explained in the HR system due to the pencils of PD and saddle-node bifurcations that are generated at homoclinic codimension-two points and destroyed in other ones (see[10] for the complete bifurcation structure).

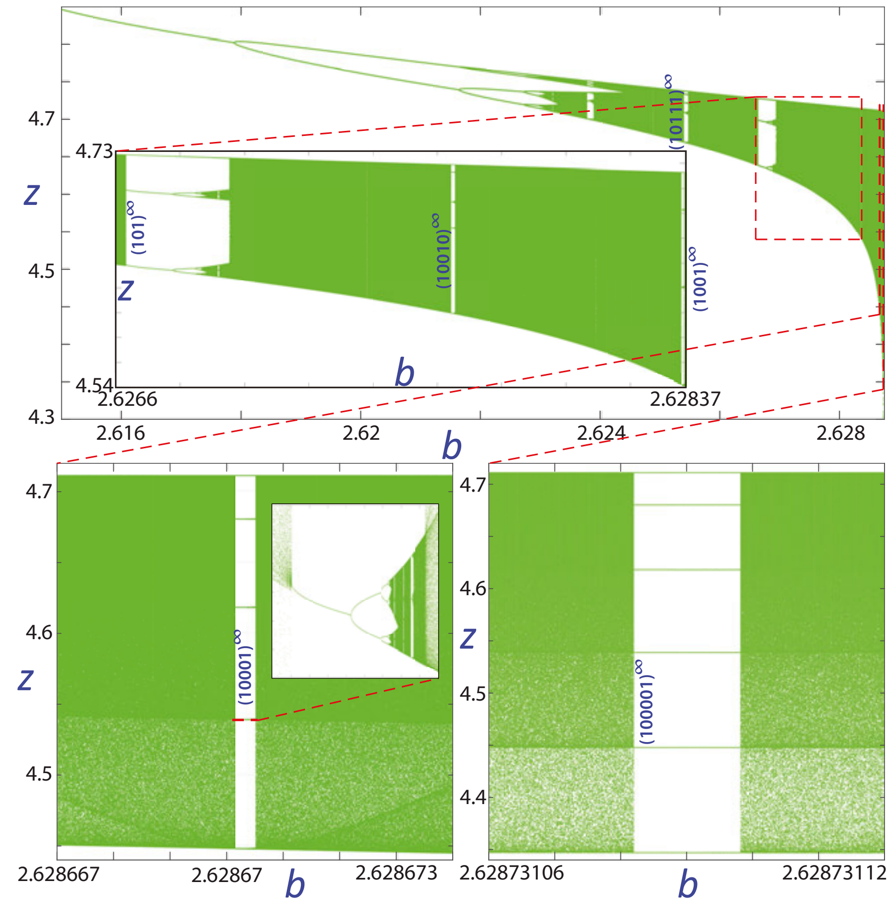

FIG. 16. Magnifications of the bifurcation diagram for the left region of the interval analyzed in Figure 15(b) (blue arrow region). The different magnifications show how the creation process on the left is the same as on the right but with opposite direction (paired period-doubling and period-halving cascades).

From Figure 15(b) we see how the interval where a periodic orbit exists is inside the intervals of the previously created orbits (some of them delimited by the dashed pink curves). That is, the intervals of existence are nested. The more interior is the interval, the more periodic orbits exist on it. Furthermore, we see that the left ends of the intervals are very close to each other (in fact they are exponentially close because all the bifurcation curves converge to a codimension-two inclination-flip homoclinic bifurcation point[10]). This is interesting from a biological point of view since small changes in the parameters generate important changes in the dynamics of the system. However, it makes the analysis of bifurcations in that area more difficult. For this reason, in Figure 16 we show several magnifications of the bifurcation diagram of Figure 15(b) for the left interval (pointed by a blue arrow) where we have located the corresponding main stability windows commented for the right area of the interval shown in Figure 9. Again, due to the very small size of some of these windows in this left area, the invariant coordinate θ of the basic orbit of the window has been useful to locate the different periodic windows. Note that without the use of this technique combining the invariant coordinate θ, it is difficult to locate the intervals of interest due to their very small size. In the figure we can see that, in fact, despite the scale of the windows being different, the order (in opposite direction) in which the periodic orbits appear is the same as described in the previous sections for the right hand side.

In Figure 15 we also observe that the number of spike-adding processes is finite for a fixed value of the small parameter ε. Specifically, for $\varepsilon = 0.01$, 17 spike-adding processes have been detected in the square-wave bursting regime, that is, the basic periodic orbit of the last generated stability window has 18 spikes, with the basic sequence $(10^{16}1)^\infty$, which becomes $(10^{17})^\infty$ and so, sequence $(10^{17}1)^\infty$ cannot be reached for that value of ε. That is, the generation of orbits is limited to those lower than $(10^{17}1)^\infty$. To observe what happens when ε changes, we have calculated the spike-counting biparametric plot (with a grid of 1000 by 1000 points in the (b,I) plane) for four different values of the small parameter ε ($\varepsilon = 0.1$, 0.01, 0.005 and 0.001) and we have represented them in Figure 17. The global picture is qualitatively the same: in all cases when ε is small (see[12,39] for a study far from the singular limit) there are spiking (dark blue), chaotic (red) and bursting (different colors) regions forming stripes. The main difference we observe is the increment in the number of chaotic-regular strips when ε decreases (and so bursting behavior with much more spikes exists). That is, when ε decreases, the number of spike-adding processes increases. Therefore, the number of periodic orbits that are generated is greater and, with it, the number of allowed sequences. This phenomena of how the number of spike-adding processes grows has been recently explained in[12] and obeys on the way how different surfaces of homoclinic

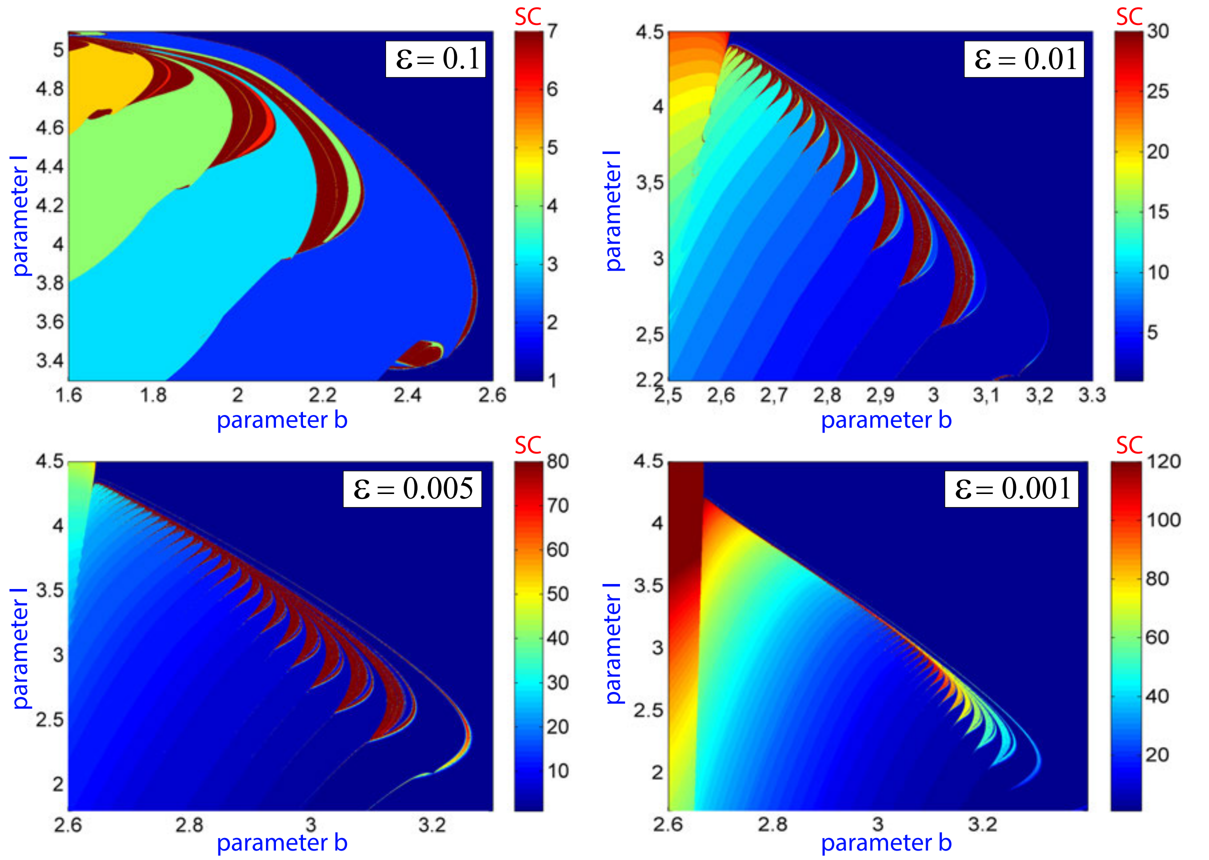

FIG. 17. (b, I)-biparametric sweeps showing the spike-counting diagram for the Hindmarsh-Rose model for different values of the small parameter ε. The color-coded bar to the right of each picture gives the corresponding spike-number range.

bifurcation surfaces are generated, and that its number grows when ε decreases.

This trend in the increase of the number of spikes for the basic orbits of certain stability windows as ε decreases can be seen in more detail in Figure 18, where a (ε, b) biparametric evolution of the number of spikes in the bursting orbit along the line $I(b) = 14.4 - 4b$ is shown. The small parameter $\varepsilon \in [10^{-2}, 10^{-4}]$ is displayed in logarithmic scale to see more clearly the exponential increment in the number of spikes. At three particular parameter values the bursting stable periodic orbit is shown. In any case, it is clear how the number of spikes grows, with a quite similar dynamics.

In summary, what we observe is that as ε approaches 0, there is a region in the parameter space where more and more symbolic sequences of the Smale template are opened. This suggests that the template is completed on the limit as more and more chaotic stripes are created in the spike-adding processes.

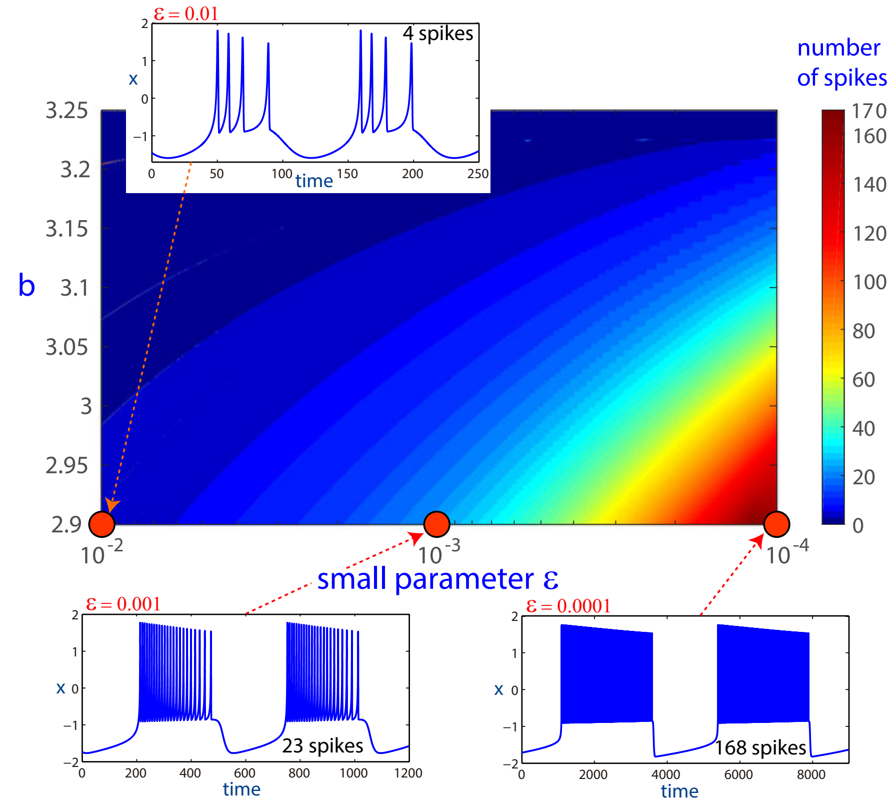

FIG. 18. (ε, b) evolution of the number of spikes in the bursting orbit along the line $I(b) = 14.4 - 4b$. The change of $\varepsilon \in [10^{-2}, 10^{-4}]$ is given in logarithmic scale to show the exponential increment in the number of spikes. The bursting orbit is shown at three particular values.

V. LEECH HEART NEURON MODEL

The previous analysis is focused on a simplified mathematical neuron model, the Hindmarsh-Rose model, in the square-wave bursting regime. In this section we show that the present analysis seems to be the general one for 3D square-wave bursters. We consider now an endogenous burster[22,40] of the Hodgkin-Huxley type[20] that describes the bursting phenomena in leech heart neurons (see[22] and references therein for an exhaustive description of the model):

$$\begin{cases} CV' = -I_{\mathrm{Na}} - I_{\mathrm{K2}} - I_{\mathrm{L}} - I_{\mathrm{app}}, \\ \tau_{\mathrm{K2}} m'_{\mathrm{K2}} = m^{\infty}_{\mathrm{K2}}(V) - m_{\mathrm{K2}}, \\ \tau_{\mathrm{Na}}\, h'_{\mathrm{Na}} = h^{\infty}_{\mathrm{Na}}(V) - h_{\mathrm{Na}}, \end{cases} \tag{7}$$

with

$$I_{\mathrm{L}} = \bar{g}_{\mathrm{L}}(V - \mathrm{E}_{\mathrm{L}}), \;\; I_{\mathrm{K2}} = \bar{g}_{\mathrm{K2}}\, m_{\mathrm{K2}}^2 (V - \mathrm{E}_{\mathrm{K2}}),$$

$$m_{\mathrm{Na}} = m_{\mathrm{Na}}^{\infty}(V), \quad I_{\mathrm{Na}} = \bar{g}_{\mathrm{Na}}\, m_{\mathrm{Na}}^3 h_{\mathrm{Na}} (V - \mathrm{E}_{\mathrm{Na}}),$$

where C is the membrane capacitance; V is the membrane potential; I_{Na} is the fast voltage gated sodium current with slow inactivation h_{Na} and fast activation m_{Na}; I_{K2} is the persistent potassium current with activation m_{K2}; I_{L} is leak current and I_{app} is a constant polarization or external applied current. The steady state values of gating variables are given by the experimentally calibrated Boltzmann functions:

$$\begin{aligned}
h_{\mathrm{Na}}^{\infty}(V) &= [1 + \exp(500(V + 0.03391))]^{-1}, \\
m_{\mathrm{Na}}^{\infty}(V) &= [1 + \exp(-150(V + 0.0305))]^{-1}, \\
m_{\mathrm{K2}}^{\infty}(V) &= [1 + \exp(-83(V - 0.02))]^{-1}.
\end{aligned}$$

The values of the fixed parameters in the model used in this paper[22] are: $\mathrm{E}_{\mathrm{Na}} = 0.045$, $\bar{g}_{\mathrm{Na}} = 200$, $\mathrm{E}_{\mathrm{K2}} = -0.07$, $\bar{g}_{\mathrm{K2}} = 30$, $\mathrm{E}_{\mathrm{L}} = -0.046$, $\bar{g}_{\mathrm{L}} = 8$, $C = 0.5$ and $\tau_{\mathrm{Na}} = 0.0405$.

There is a principal parameter controlling the activity in the model of the individual burster: the magnitude of the external current I_{app} that affects the fast voltage dynamics, and we also consider the parameter τ_{K2}. Both I_{app} and τ_{K2} are independent bifurcation parameters. Their variations make the neuronal dynamics evolves and transitions between tonic spiking, bursting and quiescence. Figure 19(a) represents the $(\tau_{\mathrm{K2}}, I_{\mathrm{app}})$-biparametric sweep of the neuron model using the spike-counting method[23]. One can see, in a quite similar picture as the ones shown for the Hindmarsh-Rose model, the structures separated by spike-adding bifurcations[9] with clearly demarcated regions corresponding to bursting, tonic spiking and quiescence states. A template analysis of the leech neuron model at the chaotic attractors for the selected parameter values (color circled points on the left picture, $\tau_{\mathrm{K2}} = 0.2$, 0.266 and 0.316) in the white line marked in the figure confirms that the Smale horseshoe template is still the global template in this model. Therefore, the FRM (given by the values of the local minima of V) of these chaotic attractors are unimodal giving also a symbolic description of all the orbits with just two symbols. Besides, they show the same evolution in the apparition of symbolic sequences as the Hindmarsh-Rose model.

In Figure 20 we show on the (a),(c) and (e) plots the chaotic attractor projections on the plane (y,z) for the selected parameter values. On the (b),(d) and (f) plots we show time series of the different attractors showing the symbolic sequence. As in the Figure 13 we use different colors to indicate different evolution on the symbolic sequence for the chaotic orbit: *Blue* color is related

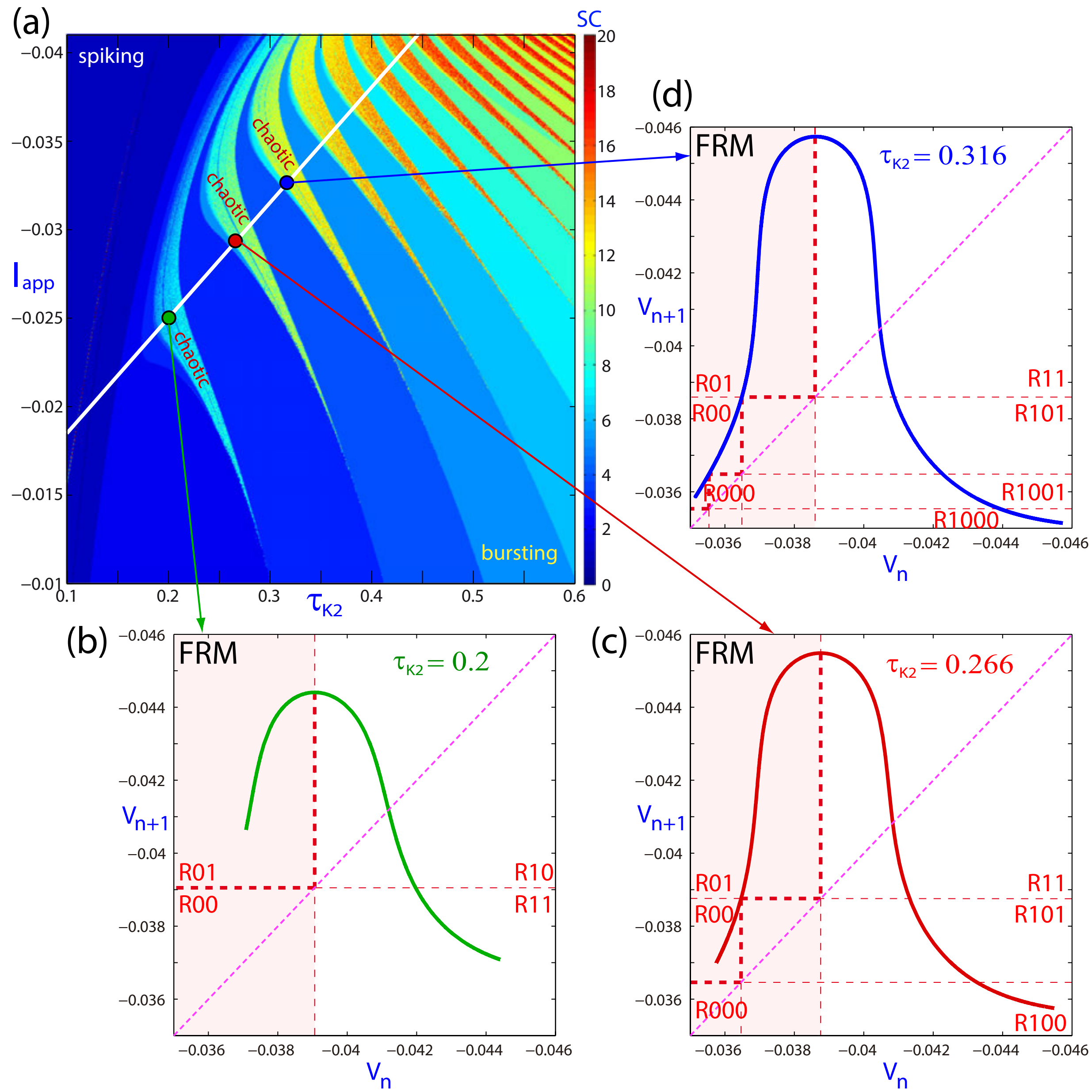

FIG. 19. (a): (τ_{K2}, I_{app})-biparametric sweep of the leech heart neuron model (7) based on the spike-counting approach. The color-coded bar on the right gives the spike-number range. (b)-(d): FRM of the chaotic attractors for the selected values of parameter τ_{K2} (color circled points on the biparametric picture) on the white line $I_{app}(\tau_{K2}) = -0.065\tau_{K2} - 0.012$.

641 with a loop that goes from a symbolic value 0 to 1, *green* from 1 to 0, *brown* from 1 to 1 and *red* 642 from 0 to 0. When $\tau_{K2} = 0.2$ the chaotic attractor has forbidden the chain 0 to 0, and so the red 643 color is not present. In the case $b = 0.266$, the chaotic attractor has opened a new sequence, 0 to 644 0 (*red* color). Finally, when $\tau_{K2} = 0.316$ more '0' chains are allowed. This process is the same

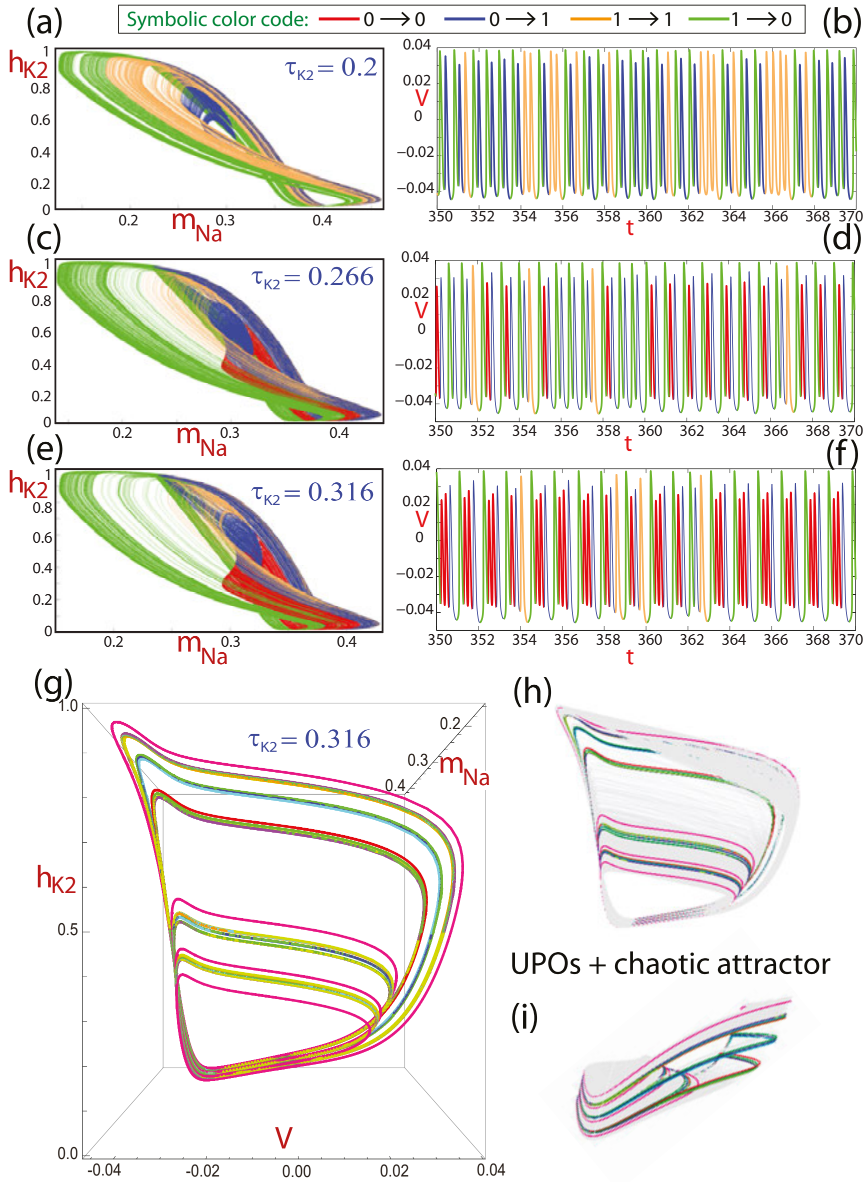

FIG. 20. Top left ((a),(c),(e) plots): Chaotic attractor projections on the plane (y,z) for the selected parameter values of the leech heart neuron model. Different colors indicate different evolution on the symbolic sequence for the chaotic orbit. Top right ((b),(d),(f)): time series of the different attractors showing the symbolic sequence. We can see a similar situation to that observed with the chaotic attractors of HR model. Bottom ((g),(h),(i)): three views of the chaotic attractor and low multiplicity UPOs for $\tau_{K2} = 0.316$.

for all the chaotic attractors along the spike-adding process and it is exactly the same situation as observed for the HR model in Section IV B. The bottom plots ((g),(h) and (i)) present three views of the chaotic attractor and the UPOs of low multiplicity for $\tau_{K2} = 0.316$ to show their spatial

PLEASE CITE THIS ARTICLE AS DOI: 10.1063/5.0043302

distribution.

Finally, we remark that the leech heart neuron model is directly based on the Hodgkin-Huxley model, and a large plethora of neuron models nowadays follows a similar model. Therefore, this section has shown that a quite similar phenomenon is expected to happen in numerous neuron models with square-wave bursting behavior and so the Smale topological template and the orderly generation of symbolic sequences at the chaotic spike-adding process seems to be a quite generic process.

VI. DISCUSSION: GLOBAL SCENARIO

The main goal of this article is to provide a complete and didactic panorama of the organization of the chaotic invariant sets in square-wave neuron models, joining different techniques and linking the recent results on the bifurcation analysis on this kind of systems. The new results here presented, and the previous ones, show us the complex but completely organized structure of the set of periodic orbits embedded in the chaotic invariant sets, and how the spike-adding phenomena allow increasing such complexity. This article details all this process connecting symbolic dynamics and bifurcation theory.

In previous articles in literature[9–11,24] it has been detected that in different neuron models there is a region with square-wave bursting where stripes of dominant chaotic behavior alternate with others of a periodic type. In addition, these stripes are structured in the form of onion layers. Therefore, a point in the parametric space that falls within the region determined by a layer is also inside the previous layers. Providing a graphical summary, in Figure 21 we show the global theoretical scheme[9,10] of the organization of the chaotic regions in this "onion-like", and the location of some of the bifurcations associated to the creation of this scheme. The straight black line is the homoclinic bifurcation line (note that in fact it is a double line as the homoclinic bifurcation curve folds itself on the right side[10,11]), and the straight blue line is the selected line where a deeper numerical study has been done in this article. This line crosses all the interesting structures.

On the plot (c) we add to the classical blow-up around the orbit-flip (OF) codimension-2 bifurcation points[37] of type C the location of another countable new set of pencils of countable symbolic-flip bifurcations (SF). Each SF line appears before each PD one, allowing a new combination of symbols for the symbolic sequences associated with the different orbits. These SF lines give the option to have a new PD bifurcation allowing the creation of new periodic orbits, as new

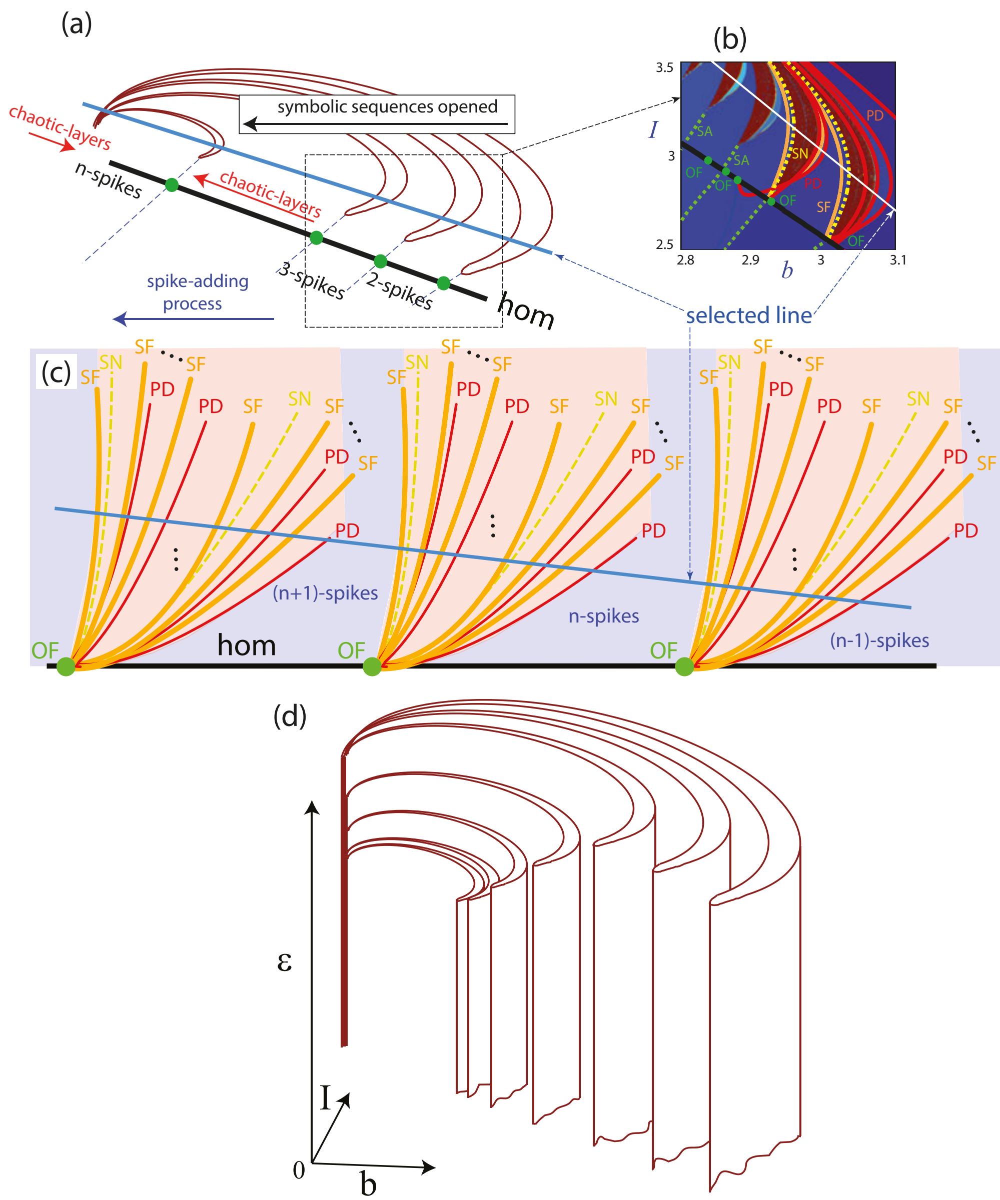

FIG. 21. Theoretical sketch of the bifurcation scenario. (a) Biparametric scheme of the "onion-like" structure of the main chaotic region[9–11]. The chaotic stripes are accumulated on the left side. The spike-adding process changes the stable periodic orbits outside the chaotic region and generates new allowed symbolic sequences. (b) Unfolding of the main bifurcation lines over the spike-counting diagram. (c) Theoretical blow-up around the Orbit-Flip (OF) codimension-2 bifurcation points. The OF points are of type C and therefore they originate countable pencils of PD and SN (of limit cycles) bifurcation lines, but also of symbolic-flip (SF) bifurcations. (d) Three-parametric scheme of the "onion-like" structure and the apparition of new spike-adding processes when ε decreases.

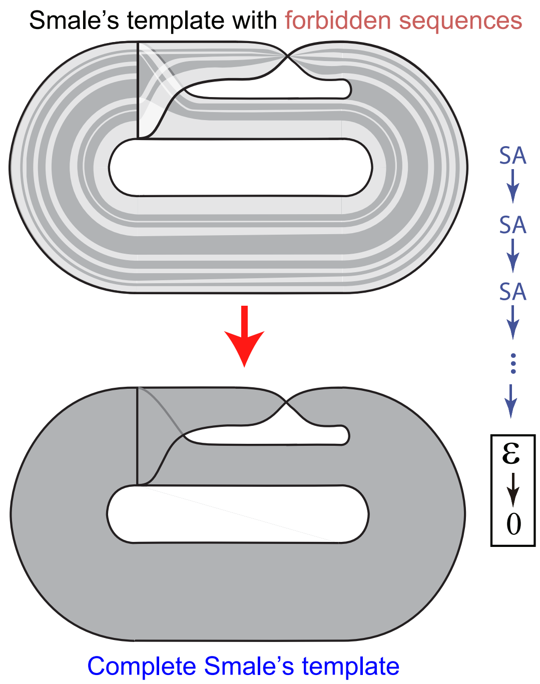

FIG. 22. The maximal topological template, with forbidden symbolic sequences at a given $\varepsilon > 0$, converges, when more and more spike-adding (SA) processes are included, towards the complete Smale topological template when $\varepsilon \searrow 0$.

symbolic sequences are permitted. We have observed that these processes are mainly grouped in the chaotic stripes between stability windows of n and $n+1$ spikes. This grouping corresponds to the so-called chaotic spike-adding process. Thus we refine with this new set of pencils of bifurcations the fine tissue of this process. We have also seen that the further we go into the layers of the onion, the more symbolic sequences are allowed in the dynamics of the system. The number of existing spike-adding layers for a specific value of the small parameter ε is finite, generating that not all possible symbolic sequences are allowed for specific values of the parameters. Thus, the topological template of the chaotic invariant set does not completely fill the Smale template, being a subtemplate with a Cantor type structure with gaps left by the forbidden sequences.

Figure 21(d) sketches the three-parametric scheme of the chaotic "onion-like" structures, showing how, when ε grows, less and less of these structures are present. The reason of this phenomenon is explained in detail in[10] where it is shown how the primary homoclinic bifurcation surfaces, where the codimension-two bifurcation points are located and therefore where the bifurcations are generated, disappear one by one when ε grows.

Therefore, considering all the results shown in the article, it is possible to conjecture that (see

Figure 22) the topological template converges when $\varepsilon \searrow 0$ to the complete Smale template with all symbolic sequences allowed, and therefore, with all associated UPOs. This result provides a nice global organization of the structure of the chaotic invariant sets showing that closer to the "center" of the onion-like structure and with a smaller value of the small parameter, more and more symbolic sequences are opened and the topological template is more complete.

VII. CONCLUSIONS

In this paper we have studied, for square-wave bursting neuron models, the evolution of the chaotic invariant set along the three-parameter region where the chaotic spike-adding studied by Terman[4] occurs. The basic ingredient necessary to carry out our study is to have a region of the phase space in which there is a chaotic invariant set whose FRM is unimodal. We have seen that this situation occurs both in the HR model and in a realistic leech heart neuron model (although other neuron models seem to obey the same structure). We have shown the symbiosis between the periodic orbits and the coexisting chaotic invariant set in the dynamics of these neuron models. It is widely known that the periodic orbits, once they are unstable, are incorporated into the skeleton of the chaotic invariant set, thus giving shape to it. The dynamics of a point within the chaotic set will be conditioned by the constant visit of neighborhoods close to these unstable orbits. In this paper we also show how the chaotic invariant set conditions these periodic orbits before they are even absorbed by the chaotic invariant set.

Specifically, we have seen how the simple grammar defined with two symbols from the unimodal FRM of the chaotic invariant has allowed us to assign symbolic sequences to all the orbits of the system. The ordering of the symbolic sequences associated with the different orbits determines an analogous ordering in the appearance (and disappearance) of these sequences (and therefore of the corresponding periodic orbits) in the parametric space. This ordering in the parametric space, and the region of the phase space that the chaotic set occupies, also condition the position of the periodic orbits that are generated at any parametric conditions. This influence is maintained throughout the entire parametric region in which such family of periodic orbit exists.

In addition, we have detailed the bifurcations that generate the appearance of the different symbolic sequences and their corresponding periodic orbits. We have also shown that the different bifurcations appear following an infinitely repeating general sequence. This sequence shows various levels of self-similarity. Furthermore, we have shown how the basic orbits of each stability window appear as the limit of a succession of orbits that have been previously generated. With all this we have been able to describe in fine detail the chaotic spike-adding process.

Moreover, this article shows that the topological template of the chaotic invariant sets of the neuron model is a subtemplate of the Smale topological template where some symbolic sequences are forbidden for fixed values of the small parameter, but the limit case ($\varepsilon \searrow 0$) is the complete Smale template with all symbolic sequences allowed, and therefore, with all the associated UPOs.

In summary, we have illustrated how the symbolic analysis of the existing orbits in the dynamics of the system establishes an order in the chaos that underlies said dynamics.

SUPPLEMENTARY MATERIAL

The supplementary material provides information on the stability transformation (ST) method that was used to calculate the necessary UPOs. Note that continuation techniques were also used to locate the periodic orbits. The initial conditions of these UPOs are provided. It also describes the use of successive return maps of a chaotic attractor to determine how many UPOs of a given multiplicity are foliated in it.

ACKNOWLEDGMENTS

The authors are deeply grateful to Prof. Marc Lefranc for his help in calculating the topological templates of the different chaotic attractors and for stimulating discussions on the subject. R. Barrio, M.A. Martínez and S. Serrano have been supported by the Spanish Ministry of Economy and Competitiveness (grants PGC2018-096026-B-I00 and PID2019-105674RB-I00) and European Social Fund (EU) and Aragón Government (Grant LMP124-18 and Group E24-17R).

DATA AVAILABILITY

Data available in the article or in the Supplementary Material file. The simulations have been done using the AUTO[34,35] and the TIDES[41,42] softwares.

REFERENCES

[1] P. Cvitanović, "Periodic orbits as the skeleton of classical and quantum chaos," Physica D **51**, 138–151 (1991).

[2] J. Rinzel, "Bursting oscillations in an excitable membrane model," in *Ordinary and partial differential equations (Dundee, 1984)*, Lecture Notes in Math., Vol. 1151 (Springer, Berlin, 1985) pp. 304–316.

[3] E. Izhikevich, *Dynamical systems in neuroscience. The geometry of excitability and bursting* (MIT Press, Cambridge, Mass, 2007).

[4] D. Terman, "Chaotic spikes arising from a model of bursting in excitable membranes," SIAM J. Appl. Math. **51**, 1418–1450 (1991).

[5] H. Korn and P. Faure, "Is there chaos in the brain? II. Experimental evidence and related models," C. R. Biologies **326**, 787–840 (2003).

[6] Y. Hirata, M. Oku, and K. Aihara, "Chaos in neurons and its application: Perspective of chaos engineering," Chaos **22**, 047511 (2012).

[7] R. Gilmore, X. Pei, and F. Moss, "Topological analysis of chaos in neural spike train bursts," Chaos **9**, 812–817 (1999).

[8] E. M. Izhikevich, "Neural excitability, spiking and bursting," International Journal of Bifurcation and Chaos **10**, 1171–1266 (2000).

[9] R. Barrio, M. A. Martinez, S. Serrano, and A. Shilnikov, "Macro- and micro-chaotic structures in the Hindmarsh-Rose model of bursting neurons," Chaos **24**, 023128 (2014).

[10] R. Barrio, S. Ibáñez, L. Pérez, and S. Serrano, "Spike-adding structure in fold/hom bursters," Communications in Nonlinear Science and Numerical Simulation **83**, 105100 (2020).

[11] D. Linaro, A. Champneys, M. Desroches, and M. Storace, "Codimension-two homoclinic bifurcations underlying spike adding in the Hindmarsh-Rose burster," SIAM J. Appl. Dyn. Syst. **11(3)**, 939–962 (2012).

[12] R. Barrio, S. Ibáñez, and L. Pérez, "Homoclinic organization in the Hindmarsh–Rose model: A three parameter study," Chaos **30**, 053132 (2020).

[13] M. Storace, Linaro, and E. de Lange, "The Hindmarsh-Rose neuron model: Bifurcation analysis and piecewise-linear approximations," Chaos **18**, 033128 (2008).

[14] J. S. Birman and R. F. Williams, "Knotted periodic orbits in dynamical systems I: Lorenz's equations," Topology **22**, 4–827 (1983).

[15]J. S. Birman and R. F. Williams, "Knotted periodic orbits in dynamical systems II: Knot holders for fibered knots," Contemporary Mathematics **20**, 1–60 (1983).

[16]J. Guckenheimer and R. F. Williams, "Structural stability of Lorenz attractors," Publications Mathématiques de l'IHÉS **50**, 59–72 (1979).

[17]R. Gilmore, "Topological analysis of chaotic dynamical systems," Rev. Modern Phys. **70**, 1455–1529 (1998).

[18]R. Gilmore and M. Lefranc, *The topology of chaos: Alice in Stretch and Squeezeland* (WILEY-VCH Verlag GmbH & Co. KGaA, 2011).

[19]B. Hao and W. Zheng, *Applied Symbolic Dynamics and Chaos*, 2nd ed. (World Scientific, 2018).

[20]A. L. Hodgkin and A. F. Huxley, "A quantitative description of membrane current and its application to conduction and excitation in nerve," J. Physiol. **117**, 500–544 (1952).

[21]J. L. Hindmarsh and R. M. Rose, "A model of the nerve impulse using three coupled first-order differential equations," Proc. Roy. Soc. Lond. **B221**, 87–102 (1984).

[22]A. Shilnikov, "Complete dynamical analysis of a neuron model," Nonlinear Dynamics **68**, 305–328 (2012).

[23]R. Barrio and A. Shilnikov, "Parameter-sweeping techniques for temporal dynamics of neuronal systems: case study of Hindmarsh-Rose model," Journal of Mathematical Neuroscience **1**, 6 (2011).

[24]R. Barrio, M. Lefranc, M. A. Martínez, and S. Serrano, "Symbolic dynamical unfolding of spike-adding bifurcations in chaotic neuron models," EPL (Europhysics Letters) **109**, 20002 (2015).

[25]H. Kantz and P. Grassberger, "Repellers, semi-attractors, and long-lived chaotic transients," Physica D **17**, 75–86 (1985).

[26]J. Milnor and W. Thurston, "On iterated maps of the interval," Lecture Notes in Mathematics **1342**, 465–563 (1988).

[27]G. Boulant, M. Lefranc, S. Bielawski, and D. Derozier, "A nonhorseshoe template in a chaotic laser model," Int. J. Bifurcation Chaos **8**, 965–975 (1998).

[28]G. B. Mindlin, H. G. Solari, M. A. Natiello, R. Gilmore, and X.-J. Hou, "Topological analysis of chaotic time series data from Belousov–Zhabotinski reaction," J. Nonlinear Sci. **1**, 147–173 (1991).

[29]Z. Arai, "A rigorous numerical algorithm for computing the linking number of links," Nonlinear Theory and Its Applications, IEICE **1**, 104 (2013).

[30]M. Rosalie and C. Letellier, "Systematic template extraction from chaotic attractors: I. genus-one attractors with an inversion symmetry," J. Phys. A: Math. Theor. **46**, 375101 (2013).

[31]J. Plumecoq and M. Lefranc, "From template analysis to generating partitions. I. Periodic orbits, knots and symbolic encodings," Phys. D **144**, 231–258 (2000).

[32]J. Plumecoq and M. Lefranc, "From template analysis to generating partitions. II. Characterization of the symbolic encodings," Phys. D **144**, 259–278 (2000).

[33]P. Holmes, "Bifurcation sequences in horseshoe maps: Infinitely many routes to chaos," Physics Letters A **104**, 299–302 (1984).

[34]E. Doedel, "AUTO: a program for the automatic bifurcation analysis of autonomous systems," in *Proceedings of the Tenth Manitoba Conference on Numerical Mathematics and Computing, Vol. I (Winnipeg, Man., 1980)*, Vol. 30 (1981) pp. 265–284.

[35]E. J. Doedel, R. Paffenroth, A. R. Champneys, T. F. Fairgrieve, Y. A. Kuznetsov, B. E. Oldeman, B. Sandstede, and X. J. Wang, "Auto2000," http://cmvl.cs.concordia.ca/auto.

[36]B. Derrida, A. Gervois, and Y. Pomeau, "Iteration of endomorphisms on the real axis and representation of numbers," Annales de l'I.H.P. Physique Théorique **29**, 305–356 (1978).

[37]A. J. Homburg and B. Sandstede, "Homoclinic and heteroclinic bifurcations in vector fields," Handbook of dynamical systems **3**, 379–524 (2010).

[38]E. Sander and J. A. Yorke, "Connecting period-doubling cascades to chaos," International Journal of Bifurcation and Chaos **22**, 1250022 (2012).

[39]R. Barrio, S. Ibáñez, and L. Pérez, "Hindmarsh-Rose model: Close and far to the singular limit," Physics Letters A **381**, 597 – 603 (2017).

[40]J. Wojcik, R. Clewley, and A. Shilnikov, "Order parameter for bursting polyrhythms in multifunctional central pattern generators," Phys. Rev. E **83**, 056209 (2011).

[41]A. Abad, R. Barrio, F. Blesa, and M. Rodríguez, "TIDES web page: `https://sourceforge.net/projects/tidesodes/`," (2011).

[42]A. Abad, R. Barrio, F. Blesa, and M. Rodríguez, "TIDES: a Taylor Integrator for Differential EquationS," ACM Transactions on Mathematical Software **39**, 5:1–5:28 (2012).